Compaction-driven fluid flow in viscoelastic rock

Article *in* Geodinamica Acta · March 1998

DOI: 10.1016/S0985-3111(98)80006-5

CITATIONS
181

READS
119

2 authors, including:

James Alexander Denis Connolly
ETH Zurich
223 PUBLICATIONS **11,851** CITATIONS

SEE PROFILE

Geodinamica Acta (Paris) 1998, 11, 2-3, 55–84

Compaction-driven fluid flow in viscoelastic rock

J.A.D. Connolly* and Yu. Yu. Podladchikov

Department of Earth Sciences, ETH-Zentrum, Sonneggstrasse 5, CH-8092 Zurich, Switzerland

(Received 24 June 1997; accepted 22 December 1997)

Abstract – Compaction driven fluid flow is inherently unstable such that an obstruction to upward fluid flow (i.e. a shock) may induce fluid-filled waves of porosity, propagated by dilational deformation due to an effective pressure gradient within the wave. Viscous porosity waves have attracted attention as a mechanism for melt transport, but are also a mechanism for both the transport and trapping of fluids released by diagenetic and metamorphic reactions. We introduce a mathematical formulation applicable to compaction driven flow for the entire range of rheological behaviors realized in the lithosphere. We then examine three first-order factors that influence the character of fluid flow: (1) thermally activated creep, (2) dependence of bulk viscosity on porosity, and (3) fluid flow in the limit of zero initial connected porosity. For normal geothermal gradients, thermally activated creep stabilizes horizontal waves, a geometry that was thought to be unstable on the basis of constant viscosity models. Implications of this stabilization are that: (1) the vertical length scale for compaction driven flow is generally constrained by the activation energy for viscous deformation rather than the viscous compaction length, and (2) lateral fluid flow in viscous regimes may occur on greater length scales than anticipated from earlier estimates of compaction length scales. In viscous rock, inverted geothermal gradients stabilize vertically elongated waves or vertical channels. Decreasing temperature toward the earth's surface can induce an abrupt transition from viscous to elastic deformation-propagated fluid flow. Below the transition, fluid flow is accomplished by short wavelength, large amplitude waves; above the transition flow is by high velocity, low amplitude surges. The resulting transient flow patterns vary strongly in space and time. Solitary porosity waves may nucleate in viscous, viscoplastic, and viscoelastic rheologies. The amplitude of these waves is effectively unlimited for physically realistic models with dependence of bulk viscosity on porosity. In the limit of zero initial connected porosity, arguably the only model relevant for melt extraction, travelling waves are only possible in a viscoelastic matrix. Such waves are truly self-propagating in that the fluid and the wave phase velocities are identical; thus, if no chemical processes occur during propagation, the waves have the capacity to transmit geochemical signatures indefinitely. In addition to solitary waves, we find that periodic solutions to the compaction equations are common though previously unrecognized. The transition between the solutions depends on the pore volume carried by the wave and the Darcyian velocity of the background fluid flux. Periodic solutions are possible for all velocities, whereas solitary solutions require large volumes and low velocities. © Elsevier, Paris

compaction-driven fluid flow / porosity waves / melt extraction / sediment compaction / viscoelasticity / self-propagating porosity

1. Introduction

Classical treatments of fluid flow in porous media begin with the assumption of a constant permeability matrix. However, the differences between fluid and rock pressure can be large enough in geological environments, particularly at elevated temperature, that a significant amount of dilational deformation must accompany fluid flow. Dilational deformation increases both the storage capacity of the rock matrix and the matrix permeability. The effect on storativity does not fundamentally alter the nature of fluid flow as compared to that anticipated for a rigid solid matrix. In contrast, the effect on permeability is highly nonlinear and has profound implications for the nature of fluid flow. The most important implication is that a perturbation (e.g. a seismic event or chemical reaction) to an initial regime of steady fluid flow can initiate a regime in which flow is accomplished by a surge or episodic waves of fluid-filled porosity depending on whether the rock deformation is elastic or viscous, respectively. Although the wave propagated character of fluid flow in deformable media has been recognized for some time, previous investigations have considered either purely elastic [1] or purely viscous [2–4] deformation. These formulations are useful for restricted problems but cannot be used to study the entire spectrum of behaviour within

* Correspondence and reprints

the earth's lithosphere, which is dominated by elastic deformation at the surface but becomes increasingly viscous with depth [5]. Our intention here is to present a single formulation to describe fluid flow in deformable viscoelastic rocks and to classify the different types of fluid flow that can arise in geologic environments.

Compaction driven flow is of importance to understanding geological processes that involve the expulsion and migration of fluids. Problems concerning the expulsion of sedimentary pore fluids and the extraction of melts from the lithosphere have received the most attention. Although the fundamental problem is similar in both cases [6], the disparity in the approaches taken to solve these problems is remarkable. In studies of sediment compaction, it is generally assumed that the sediment can be described by an elastoplastic rheology. Because elastic deformation is reversible, this model is generally inadequate to explain natural porosity and fluid pressure distributions [7]. The role of pressure solution creep, a viscous rheology [8], in sediment compaction is well documented [9, 10]. Moreover, a simple viscoplastic compaction model can reproduce many features observed in sedimentary basins [11]. These observations provide a strong incentive for the introduction of a unified formalism for the description of compaction processes.

The instability of steady fluid flow through a deformable viscous matrix was first recognized in the geological literature as a potential mechanism for extracting melts from the lithosphere. One-dimensional models showed that the melt from a partially molten layer would be propagated in sill-like porosity waves [2–4]. Subsequently it was shown that such one-dimensional waves are unstable with respect to spherical, diapir-like waves in two and three dimensions [12–14], wave geometries that are inconsistent with dike- and sill-like natural features. This has prompted the introduction of more complex reactive transport models [15]. Results of reactive transport modelling are seductive, but the process is poorly constrained and predicated on the validity of the earlier models of viscous compaction that incorporate an oversimplification and an inappropriate initial condition. The oversimplification is that the matrix can be characterized by a constant viscosity. It is established by experiment that viscous deformation is not only dependent on porosity [16, 17], but also temperature dependent [18]. For normal geothermal gradients, a ~1–10 km decrease in depth in the lithosphere leads to a ten-fold increase in rock viscosity. We show here that this increase in viscosity stabilizes one-dimensional waves and causes them to become effectively trapped at depth unless an elastic mode of deformation is activated. The inappropriate initial condition is that there is a uniform background level of connected fluid-filled porosity throughout the rock matrix. In the context of melt transport, even if the fundamental difficulty of maintaining a pervasive melt-filled porosity at subsolidus temperatures is disregarded, the models show that steady flow is unstable. Therefore, it is difficult to envisage a process that could create the initial conditions for the model and be simultaneously consistent with the conclusions drawn from the modelling. These criticisms are less relevant to compaction models applied to sedimentary pore fluid expulsion, since aqueous fluids are thermodynamically stable at the conditions of interest and it is possible to devise realistic initial conditions for which compaction is insignificant [11]. However, it is often argued that chemical [19] or mechanical processes [20] lead to situations where pore connectivity is lost. In these situations, fluid flow induced by a diagenetic or metamorphic devolatilization reaction must propagate into a matrix with no connected porosity. The propagation of a fluid into a matrix with zero porosity is a problem that can be solved by taking into consideration the elastic properties of the matrix [21]. This fact provides additional motivation for introducing a viscoelastic rheology in the modelling of compaction-driven fluid flow.

Our formulation of the compaction equations is mathematically simple, but analytic solutions to these equations are cumbersome and not easily understood. In this paper, we therefore present numerical solutions and graphical representations of analytic solutions designed to illustrate the character of, and constraints on, compaction-driven fluid flow.

2. Mathematical formulation

The mathematical formulation employed here is for the Darcyian flow of a slightly compressible fluid through a viscoelastic matrix composed of incompressible solid grains. This formulation consists of two equations for two unknown functions, porosity (ϕ) and effective pressure (p_e, see *table 1* for additional notation)

$$\frac{1}{1-\phi}\frac{\mathrm{d}\phi}{\mathrm{d}t_\mathrm{d}} = -\frac{\phi^m}{\eta}p_\mathrm{e} - \phi^b\beta_\phi\frac{\mathrm{d}p_\mathrm{e}}{\mathrm{d}t_\mathrm{d}} \tag{1}$$

$$-\phi\beta_\mathrm{f}\frac{\mathrm{d}p_\mathrm{e}}{\mathrm{d}t_\mathrm{d}} + \frac{1}{1-\phi}\frac{\mathrm{d}\phi}{\mathrm{d}t_\mathrm{d}} = \nabla\left(\frac{k\phi^n}{\mu}(-\nabla p_\mathrm{e} - \Delta\rho g)\right) \tag{2}$$

The effective pressure is $p_e = (1-\phi)(p_s - p_f)$ and the total pressure $p_{tot} = p_s(1-\phi) + p_f\phi = p_f + p_e$ is assumed to be lithostatic such that $p_{tot} = p_{lith} = p_0 - \rho_s g z$; subscripts s, f and ϕ refer, respectively, to solid, fluid and porosity properties; ∇ is the gradient operator, $\mathrm{d}/\mathrm{d}t = (\partial/\partial t_\mathrm{d} + V_S \cdot \nabla)$ is the substantial (material) derivative relative to the solid matrix velocity; $\Delta\rho$ is the density difference $\rho_s - \rho_f$, g is gravitational acceleration; $k\phi^n$ is the matrix permeability; β_f and μ are the fluid compressibility and shear viscosity; η/ϕ^m is the matrix bulk viscosity, for which η may be depth-dependent, and $\phi^b\beta_\phi$ is the pore compressibility. For consistency with mathematical convention, we adopt a coordinate system where the depth coordinate (z) increases upward in the direction of fluid flow.

Table 1. Common symbols and characteristic parameter values.

Symbol	Meaning	Units	Value
b	porosity exponent for pore compressibility		1/2
De_f	fluid Deborah number [equation (8)]		$\phi_0\beta_f p^*$
De_ϕ	matrix Deborah number [equation (8)]		$\phi_0^b\beta_\phi p^*$
f	dimensionless porosity		ϕ/ϕ_0
f_0	initial amplitude of a flow obstruction		ϕ_1/ϕ_0
k	permeability–porosity proportionality constant	m^2	
l_η	e-fold length [equation (13), *figure 11*]	m	200–5000
m	porosity exponent for ζ		0–2
n	porosity exponent for k		3
p	dimensionless pressure [equation (5)]		$-p_e/p^*$
p^*	characteristic pressure	Pa	$\delta\Delta\rho g$
p_f	fluid pressure	Pa	
p_e	effective pressure	Pa	$p_{tot} - p_f$
p_s	solid pressure	Pa	
p_{tot}	total pressure	Pa	$p_s(1-\phi) + p_f\phi$
q	volumetric fluid flux	$m^3 \cdot m^{-2} \cdot s^{-1}$	
q_0	background volumetric fluid flux (*figure 1*)	$m^3 \cdot m^{-2} \cdot s^{-1}$	
q_1	initial flux beneath a flow obstruction	$m^3 \cdot m^{-2} \cdot s^{-1}$	
Q	creep activation energy [equation (11)]	$kJ \cdot mol^{-1}$	
t	dimensionless time		t_d / t^*
t_d	time	s	
t^*	characteristic time [equation (5)]	s	$\eta_0 / (p^*\phi_0^m)$
T	temperature	K	
V	dimensionless phase velocity		$V_\phi t^*/\delta$
V_s	matrix velocity [equation (4)]	$m \cdot s^{-1}$	
V_f	fluid velocity [equation (4)]	$m \cdot s^{-1}$	q/ϕ
V_ϕ	wave phase velocity	$m \cdot s^{-1}$	
x	horizontal distance ordinate	m	
z	depth, negative downward	m	
β_f	fluid compressibility	Pa^{-1}	$(\partial\rho_f / \partial p_f) / \rho_f$
β_ϕ	pore compressibility elastic constant	Pa^{-1}	$-(\partial\phi / \partial p_e)/\phi^b$
δ	viscous compaction length [equation (4)]	m	$\sqrt{k\eta_0\phi_0^{n-m}/\mu}$
ε	aspect ratio of a two-dimensional wave [equation (14)]		λ_x/λ_z
λ	wavelength	m	
ϕ	porosity	$m^3 \cdot m^{-3}$	
ϕ_0	background porosity (*figure 1*)	$m^3 \cdot m^{-3}$	
ϕ_1	initial porosity shock amplitude (*figure 1*)		
η	rock shear viscosity [equations (11) and (12)]	Pa·s	
η_0	η at a reference condition	Pa·s	
ζ	matrix bulk viscosity	Pa·s	η/ϕ^m
$\Delta\rho$	$\rho_s - \rho_f$	$kg \cdot m^{-3}$	
ρ_f	fluid density	$kg \cdot m^{-3}$	
ρ_r	rock density	$kg \cdot m^{-3}$	
μ	fluid viscosity	Pa·s	

Although the solid component of the matrix is incompressible, the bulk matrix is compressible because fluid may be expelled from the pore volume. Consequently, mass conservation relates the divergence of the solid velocity to the porosity production rate

$$\nabla \cdot V_s = \frac{1}{(1-\phi)}\frac{d\phi}{dt_d} \tag{3}$$

Equation (1) is the combination of equation (3) and the Maxwell volumetric strain-rate effective mean stress law for a bulk viscoelastic rheology. Equation (2) is the combined statement of Darcy's law

$$\phi(V_f - V_s) = \frac{k\phi^n}{\mu}(\nabla p_f + \rho_f g) \tag{4}$$

and fluid conservation of mass. It equates the time rate of change of fluid volume per unit volume rock to the

divergence of the fluid flux and the rate of porosity production. In the remainder of this paper, we assume that any porosity present in the matrix is connected; in the event that this is untrue, equations (1) and (2) apply only to the connected porosity within the matrix. For simplicity, the term $(1 - \phi)$ is replaced by unity and solid matrix velocity in the material derivatives is ignored ($\mathrm{d}/\mathrm{d}t \sim \partial/\partial t$). This simplification makes the formulation of equations (1) and (2) identical in Lagrangian, Eulerian and barycentric reference frames [3, 4, 22]. This approach is justified by the parameter uncertainties and by the fact that the matrix compaction velocities required by continuity are typically at least an order of magnitude less than the fluid velocity for conditions of interest. Despite this simplification, the divergence of the solid compaction velocity is properly accounted for. The present treatment differs from more complicated analyses of two-phase compaction equations [3, 4, 22] in that shear force balance consideration is not required. The viscous limit ($\beta_\phi = \beta_f = 0$) of equations 1 and 2 is mathematically equivalent to (i.e. can be reduced to) the system of equations used in viscous compaction [12, 23–25]. The elastic limit ($\eta \to \infty$) is similar to the 'mechanical' compaction models used for the sedimentary basin environment and subsurface hydrogeology [7, 26, 27]. Generalization to the plastic models is achieved by strong reduction in viscosity above a specified yield pressure.

Natural scales for non-dimensionalization of equations (1) and (2) are: the background porosity ϕ_0; the viscous compaction length $L^* = \delta$; p^* the pressure difference due to buoyancy on this length scale; and the viscous compaction time t^* (the asterisk designates the characteristic values used for non-dimensionalization)

$$L^* = \delta = \sqrt{\frac{\eta_0}{\mu} k \phi_0^{(n-m)}}$$

$$p^* = \Delta\rho g L^*$$

$$t^* = \frac{\eta_0}{p^* \phi_0^{m-1}} \tag{5}$$

Recasting equations (1) and (2) in dimensionless form yields a closed system of equations that describe the evolution of dimensionless fluid-filled porosity $f = \phi / \phi_0$ and effective pressure $p = -p_e / p^* = (p_f - p_{lith}) / p^*$

$$\frac{\partial f}{\partial t} = f^m p \tilde{\eta}(z) + f^b De_\phi \frac{\partial p}{\partial t} \tag{6}$$

$$f De_f \frac{\partial p}{\partial t} + \frac{\partial f}{\partial t} = \nabla(f^n(\nabla p - 1)) \tag{7}$$

where, in addition to the three dimensionless power law exponents n, m and b, there are three dimensionless parameters

$$De_\phi = \phi_0^{b-1} \beta_\phi \Delta\rho g L^*, \quad De_f = \beta_f \Delta\rho g L^*, \quad \tilde{\eta}(z) = \frac{\eta}{\eta_0} \tag{8}$$

The first two parameters in this list are forms of the Deborah number used in viscoelastic applications [28]. This number is the ratio of the Maxwell relaxation-time to the characteristic time of the process under investigation. As defined here, $De \ll 0$ is the viscous limit, and elasticity dominates rheological response for large $De \sim 1$. The third parameter η is the dimensionless matrix shear viscosity, which may depend on depth.

2.1. Power law exponents: n, m and b

The power-law exponents n, m and b define the dependence of the matrix permeability, bulk viscosity and pore compressibility on porosity, respectively. There is a considerable variability in the literature concerning the choice of these power law exponents. It is common practice to set some or all of them to zero for simplicity. However, setting n to zero removes an important non-linearity responsible for the formation of the porosity waves. There are strong arguments for supposing that n is near 3, a value we assume here, and not less than 2 [3, 22]. Higher values of this exponent have been determined experimentally [29], which enhance the wave-like character of fluid flow [30]. The practice of setting the rheological exponents m and b to zero is inconsistent with the common assumption that the solid grains within the matrix are incompressible, which requires that the matrix must also become incompressible in the limit $\phi \to 0$. When b is not set to zero, it is usually taken to be unity [26]. We arbitrarily adopt a value of $b = ½$. More complex treatments of poroelasticity are possible [20], but entail considerable uncertainty. Nye [16] demonstrated both experimentally and theoretically that in the limit of non-interacting pores in a viscous rheology the exponent m is unity. In more complex systems m is known to vary in the range ~½ to 2 [17]. Here we explore the dependence of the solutions to the compaction equations for $0 \leq m \leq 2$, the lower limit is taken for purposes of comparison with earlier work.

2.2. Methods

Equations (6) and (7) [or equations (1) and (2)] were solved simultaneously by Crank–Nicolson and alternating direction implicit finite difference schemes [31] for one- and two-dimensional numeric calculations, respectively. For these calculations, the surface and basal boundary conditions were $p_e = 0$ and $\partial p_e / \partial z = 0$. Lateral symmetry (no-flow) boundary conditions were imposed for the two-dimensional numerical calculations. Stationary solutions of equations (6) and (7) in a coordinate system moving with velocity V_ϕ were obtained by replacing partial time derivatives by $-V_\phi \mathrm{d}/\mathrm{d}z$.

3. Initial conditions and nomenclature

The existence of wave solutions to equations (1) and (2) in the limit of a viscous matrix is well documented [23]. The necessary conditions for these solutions are that: (1) $dk/d\phi$ is a strongly increasing function of porosity, a condition likely to be met in most geological environments; and (2) the existence of an obstruction to compaction driven flow. Such an obstruction may be simply the relatively low porosity rock overlying a chemical source of fluid-filled porosity, i.e. a devolatilization or melting reaction.

We begin by considering two one-dimensional initial porosity distributions (*figure 1*) in a matrix of constant shear viscosity that leads to the initiation of waves: (1) a step-like increase in porosity with depth between two infinite regions of constant porosity ($\phi_1 > \phi_0$); and (2) a local, sill-like, region of elevated porosity (ϕ_1) with a background porosity (ϕ_0). It is sometimes convenient to characterize these distributions by the associated excess volume, i.e. the volume of fluid-filled porosity above the background level (*figure 1*). The initial conditions for pressure are zero effective pressure throughout the porosity.

The step-like porosity distribution (infinite excess volume) is relevant to problems such as the extraction of mantle melts in which compaction drives fluid flow from a relatively large region, compared to the viscous compaction length scale. The sill-like domain of elevated porosity (finite excess volume) is relevant to situations such as might be created by a diagenetic or metamorphic devolatilization reactions or localized melting. If the step- and sill-like porosity distributions propagate with unchanging form, conservation of mass requires that the discontinuities propagate with velocity

$$V_\phi = \frac{q_1 - q_0}{\phi_1 - \phi_0}. \tag{9}$$

More generally, it is to be expected that the original porosity distribution will evolve in a complex way with

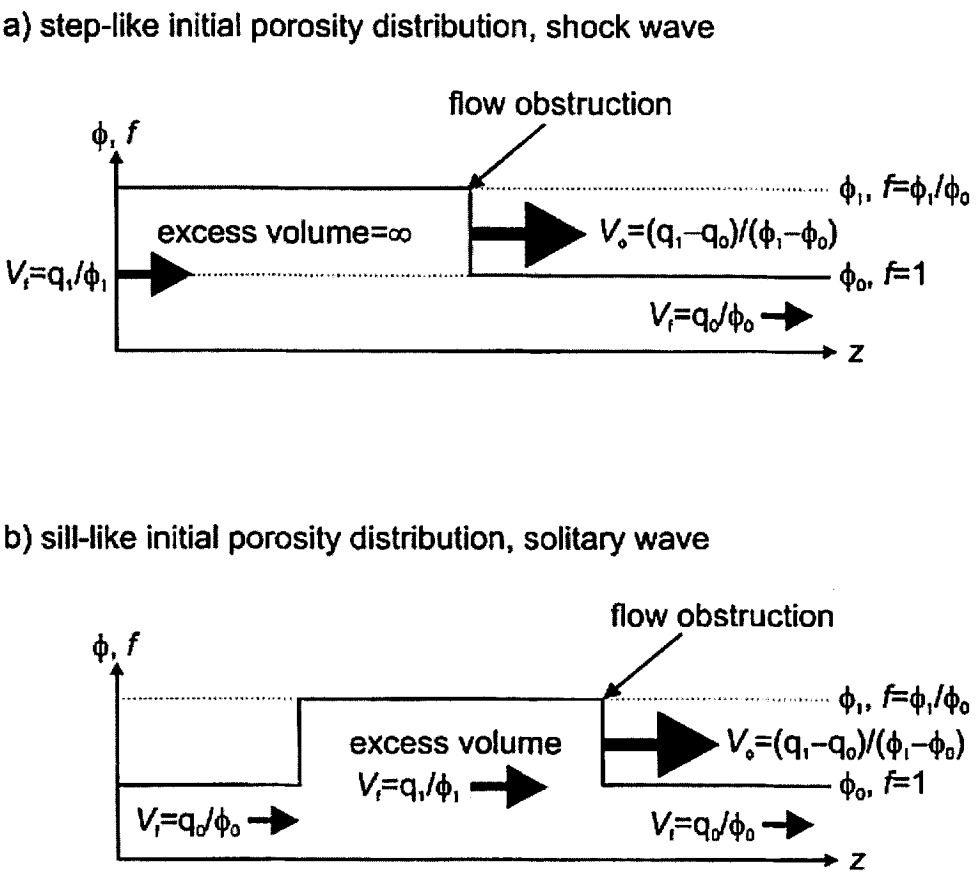

Figure 1. Initial porosity distributions and fluid velocities for one-dimensional transient models. If the distributions propagate with unchanging form they are classified as a stationary shock (a), and solitary (b) waves. For the step-like distribution, the flow obstruction separates infinite half-spaces. Stationary shocks solutions to the compaction equations are possible for an elastic matrix [1, 35], whereas solitary solutions are possible in a viscous matrix [2, 23].

time. To describe this evolution we adopt the following nomenclature.

- A shock wave is a distribution that propagates connecting to distinct levels of porosity; within this distribution there may be smaller wave-like structures that also have the character of shocks.
- A solitary wave is an isolated distribution that propagates between two nodes at the background porosity and in which the fluid flux is identical to the background flux at the wave nodes.
- Periodic waves are a distribution that propagates with nodes at a constant level above the background porosity, and in which the fluid flux at the wave nodes is different from the background value.

If a wave propagates with unchanging form, then it is stationary, otherwise it is transient. In the stationary limit (*figure 1*), the step-like initial porosity distribution propagates as a shock wave, whereas the sill-like distribution propagates as a solitary wave. In both cases, the velocity given by equation (9) is the phase velocity of the wave. For compaction-driven fluid flow, except in the limit of zero background porosity, the phase velocity is greater than the fluid velocity (q/ϕ) within the wave.

4. Step-like initial porosity distribution, viscous shocks

The immediate effect of a step-like flow obstruction in a viscous matrix (*figure 2a*) is to raise the fluid pressure near the obstruction (*figure 2b*), which results in negative effective pressures, pore dilation, and increasing permeability. Because the fluid flux within the dilated region beneath the obstruction must be less than in the deeper undeformed rocks Darcy's law requires that the fluid pressure gradient must relax toward hydrostatic conditions within the dilated region. Pore fluid pressures within this region must rise until the rate of pore dilation exceeds the rate of fluid supply from the undeformed matrix. The effective pressures at the base of the dilated region then become positive and this causes the porosity to collapse (*figure 2c*). The net result of pore dilation beneath the obstruction is to propagate the region of dilated porosity upward; while simultaneously the collapse of porosity propagates information about the obstruction backward, against the direction of flow [32]. The newly formed obstruction causes the process to repeat at greater depth relative to the shock front. The effect of this process is to create a series of wave-like structures within a large shock. Spiegelman [32] showed that for porosity exponents $m = 0$ and $n = 3$ there is no stationary solution to the compaction equations, and that the transient solution consists of a series of structures with diminishing amplitude behind the shock front (*figure 3*). With time the amplitude and velocity of the initial shock approaches, but remains less than, the velocity and amplitude of a solitary wave [23, 32]. Thus, in idealized models, the waves do not separate from the shock and the shock is constrained to have relatively small amplitudes. In principle, wave detachment could occur when the fluid flux between the shock front and the subjacent structure drops to the value of the fluid flux within the obstruction, whereupon the shock front would propagate as a solitary wave (*figure 2d*). Khodakovskii et al. [25] considered models in which additional mechanisms permit detachment of large amplitude waves. We note that heterogeneities within the background porosity would be adequate to destabilize the shock and cause detachment.

Geological application of viscous compaction models to melt extraction has generally been concerned with the extraction of a few volume percent melt from the mantle. In this context, it has been argued that shocks generated by melting are small relative to the background porosity and, therefore, an ineffective mechanism for melt extraction [25]. However, the magnitude of the model background porosity is subject only to an artificial constraint, introduced to keep compaction lengths on a scale such that viscous compaction would produce geologically relevant results. There is little physical necessity or justification for this constraint. In the limit that there is no interconnected melt-filled porosity above a partially molten layer the magnitude of the shock produced by partial melting becomes infinite (i.e. $\phi = 1$). For small, but finite background porosity, the amplitude of the wave-like structures generated for large obstruction amplitudes appear to have no asymptotic limit (*figure 4*). Thus, although these solutions are valid, they are physically unrealistic because of the extreme transient variation in effective pressure within the shock. In real systems, these variations would increase the importance of elastic deformation. Thus, a viscoelastic model for the matrix deformation is the simplest model that can describe the physics of fluid flow for the entire range of porosities realized in the natural environments.

In the limit of the small background porosity ($\phi_1 >> \phi_0$), the compaction length scale must be defined from the properties of the matrix beneath the obstruction. Thus, the practice of defining compaction length scales on the basis of the background porosity is only valid for relatively low amplitude obstructions.

5. Sill-like initial porosity distribution, viscous solitary and periodic waves

The essential difference between the evolution of the sill- and step-like porosity distributions is that in the former the source of the flux is exhaustible, although both distributions have the same initial flux behind the upper flow obstruction. Thus, the fluid flux between the wave-like structures that develops from a sill-like distribution falls more rapidly and is not constrained to approach the background flux asymptotically. Consequently, solitary or periodic waves may detach from the

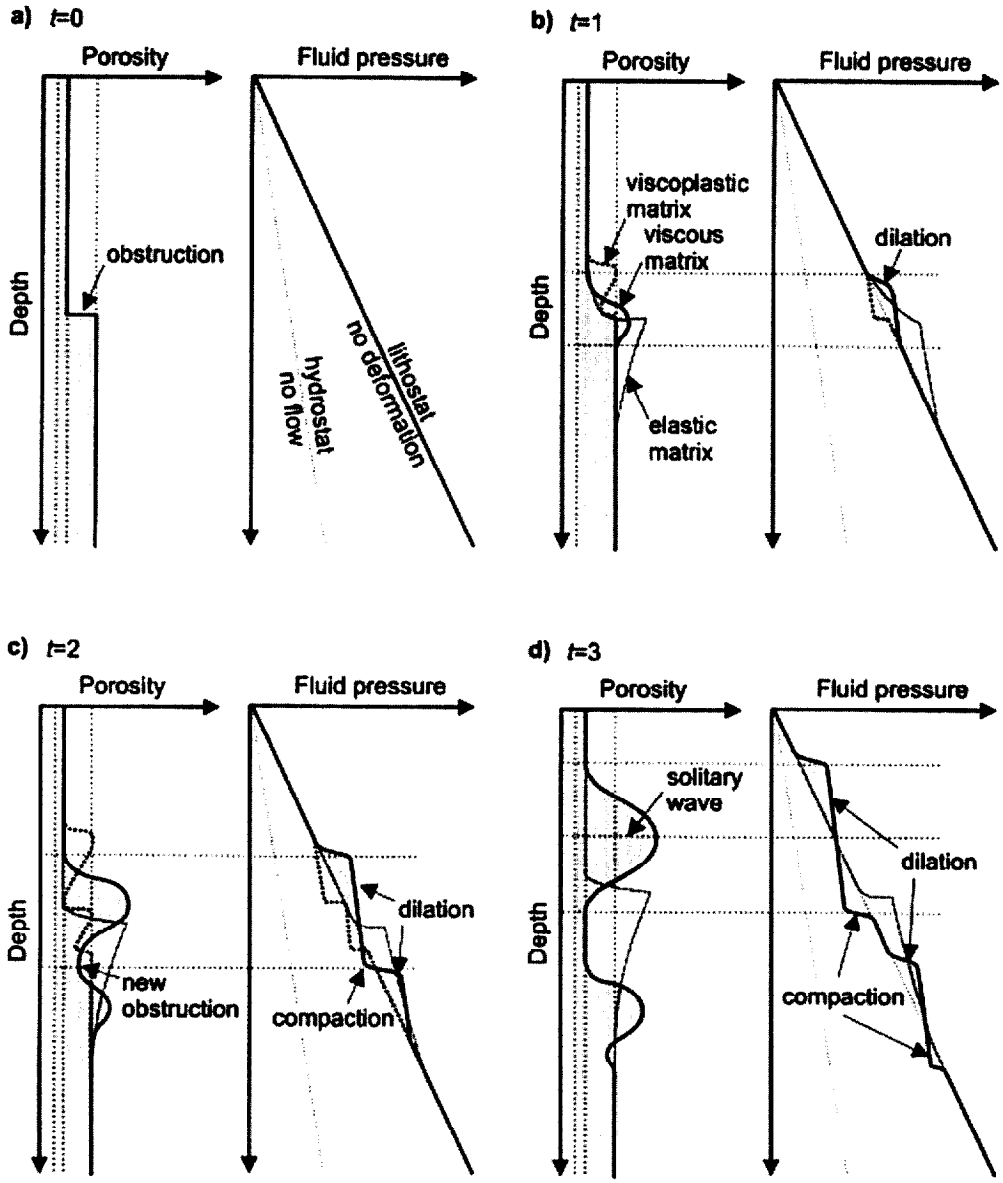

Figure 2. Schematic porosity and pressure–depth profiles illustrating the evolution and propagation of porosity waves through a low porosity obstruction in a viscous matrix (heavy solid curves). **a**. The obstruction is introduced at $t = 0$, effective pressures are initially zero. **b**. Fluid pressure rises about the obstruction, causing pore dilation and increasing permeability. Fluid flux in this region must be less than in the underlying rocks; thus, the fluid pressure gradient relaxes toward hydrostatic conditions. **c**. Fluid overpressure grows in proportion to the depth of dilation. Once the rate of pore volume increase exceeds the rate of fluid supply, the underlying porosity becomes underpressured and collapses. Porosity collapse initiates a second flow obstruction. **d**. If the porosity collapses to the value of the initial obstruction, fluid fluxes into and out of the high porosity domain are comparable and the domain propagates, by dilation and compaction, through the obstruction as a solitary wave. Solitary wave velocities must be greater than the simple shock velocity [equation (9)]. The stationary solitary wave shape is such that the total amount of pore dilation is equal to the total amount of compaction. If the matrix properties do not vary with either depth or effective pressure, the wave is symmetric. If a small, but finite, negative effective pressure is necessary to induce plastic yielding (viscoplastic rheology, heavy dotted curves in *b* and *c*), porosity waves evolve in a manner analogous to the viscous case. However, in the viscoplastic matrix, the waves are smaller, asymmetric and propagate more rapidly. In an elastic matrix (thin dotted lines), fluid pressure rises until pore dilation above the obstruction becomes comparable to the rate of fluid supply. The obstruction then propagates into the overlying matrix *c*. In contrast to Rice's solution [1], the stationary shock amplitude decays to the initial amplitude of the shock because fluid must accumulate beneath the obstruction until the fluid pressure reaches a value [equation (16)] adequate to propagate the shock. However, conservation of mass requires the same propagation velocity [equation (9)] for both solutions.

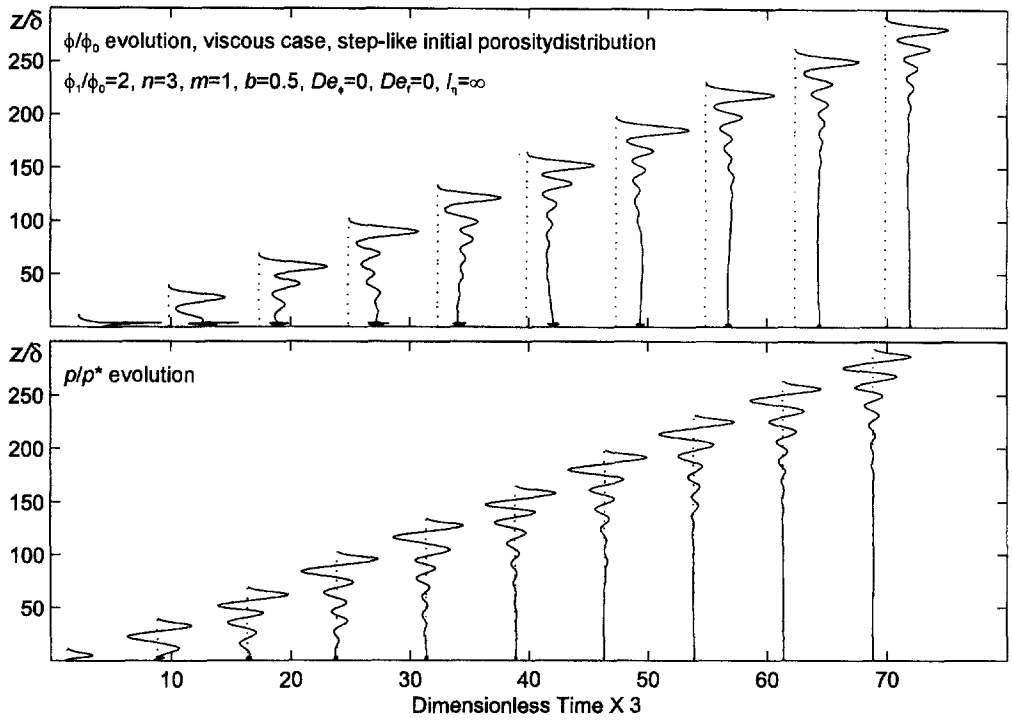

Figure 3. Transient depth ($-z$) profiles showing evolution of porosity and fluid pressure anomalies ($-p_s = p/p^*$) resulting from a small amplitude, $f_0 = 2$, step-like shock (*figure 1a*) in a viscous matrix ($n = 3$, $m = 1$, $De_\phi = 0$, $b = 0.5$, $De_f = 0$, $l_\eta = \infty$). Dotted vertical lines locate the zero-baseline for the profiles as a function of time. Profiles are scaled such that a unit dimensionless porosity (f) or dimensionless pressure is identical to 4 units of dimensionless time. Spiegelman [32] demonstrated that for a small shock of initial amplitude $f_0 = 2$ and the rheological exponent $m = 0$, the transient shock front asymptotically grows to a maximum amplitude of $f = 4$. The present calculation for $f_0 = 2$ and $m = 1$, suggests an asymptotic limit of ~2.6 f_0. Noise at the lower boundary of the porosity and pressure profiles, and profiles for subsequent transient one-dimensional models, is an artifact. The noise is a consequence of the unconstrained effect of pressure gradients at the lower boundary in these calculations. The noise is cosmetic and has no impact on the model evolution.

initial region of excess volume and propagate independently of it, provided there is a finite background flux.

After the initial discovery of the relevance of viscous porosity waves to geological processes, the classification of porosity waves was the subject of considerable discussion. However, periodic wave solutions to the compaction equations (*figures 5* and *6*) were not previously recognized. The condition for the transition from periodic to solitary solutions is related to the velocity of the background flux and the total excess volume available to form waves. Periodic solutions are possible for all velocities, but solitary solutions require large excess volumes and low velocities (*figure 6*). This is verified by transient numerical calculations in which the initial waves that detach from a shock are very nearly solitary, but the residual porosity propagates as periodic waves (*figure 7*). If the initial extent of the region of elevated porosity is small (~δ), all the porosity in excess of the background porosity may be carried by a single solitary wave.

Viscous waves typically develop on the length scale greater than, but comparable to δ (*figure 8*). The remaining characteristics of the waves are remarkably sensitive to model parameters (*figures 8* and *9*). However, in the limit of large porosity waves for $m = 1$, stationary solutions have essentially Gaussian porosity distributions [30]. This can be shown analytically given the observation that, in the vicinity of a porosity maximum at $z = 0$, $p \approx \Delta\rho g z$ and therefore $-V_\phi(\mathrm{d}\phi/\mathrm{d}z) \approx \phi\Delta\rho g z/\eta$, for which the analytic stationary solution is

$$\phi = \phi_{\max}\exp\left(-\frac{\Delta\rho g}{2\eta}\frac{z^2}{V_\phi}\right) \tag{10}$$

A potential application of this limit is in the description of the compaction front that defines the lithostatic-hydrostatic fluid pressure transition in sedimentary basins. This front can be characterized as the lower half of a stationary porosity wave, numerical calculations based on this model reproduce natural porosity distributions (*figure 10*).

6. Porosity waves in a viscoplastic matrix

A characteristic feature of viscous porosity waves is that the mean effective pressure within the wave is near

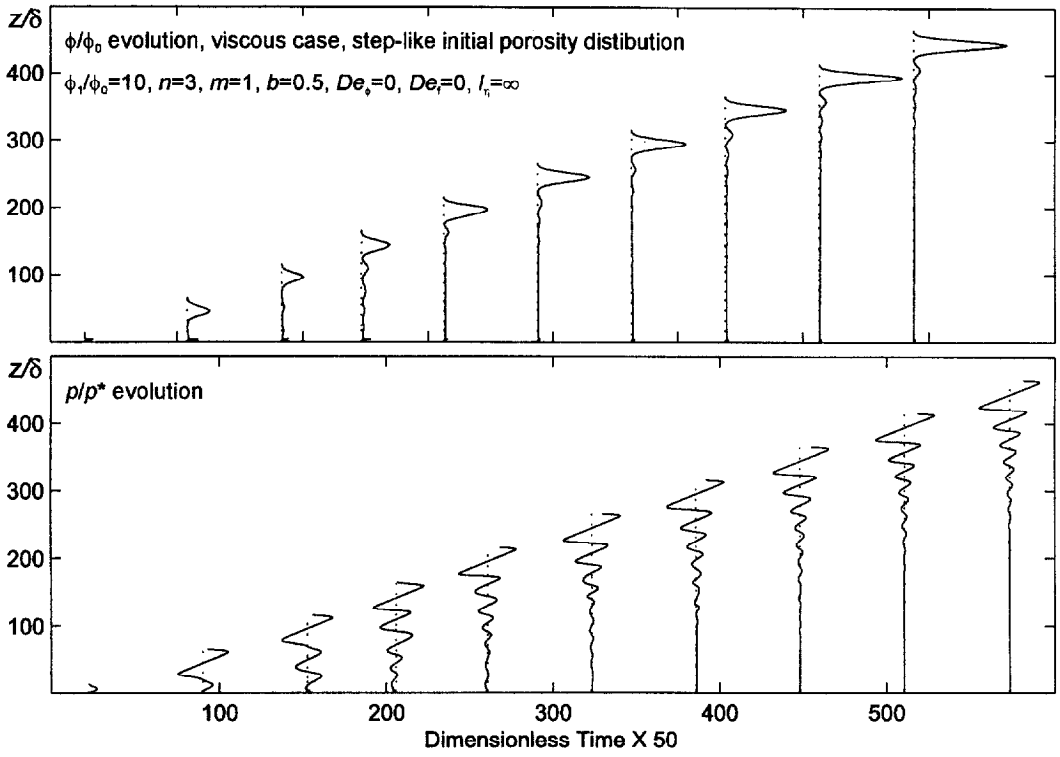

Figure 4. Transient depth ($-z$) profiles showing evolution of porosity and fluid pressure anomalies ($-p_e$) for a step-like shock in a viscous matrix ($f_0 = 10$, $n = 3$, $m = 1$, $De_\phi = 0$, $b = 0.5$, $De_f = 0$, $l_\eta = \infty$) with initial amplitude $f_0 = 10$. The profiles are scaled such that a unit dimensionless porosity (f) or dimensionless pressure is identical to 50 units of dimensionless time. The calculation demonstrates that the amplitude of the transient shock is essentially unlimited if the initial shock is not small (i.e. $f_0 \sim 1$). Despite the large amplitude of the shock front, solitary waves do not detach from the shock, however detachment might be initiated by heterogeneities in the background porosity.

zero; therefore, large negative effective pressures may be generated in the upper portions of such waves. Rocks are unable to sustain significant negative effective pressures because they fail plastically under moderate tensile stress, particularly at shallow depth [5]. It can be argued that this consideration justifies dismissing viscous waves, which are propagated by negative effective pressures, as a possible mechanism of fluid flow [11]. However, the rate of propagation of plastic dilational deformation is limited by the rate at which viscous compaction can drive fluid flow to the region where dilation occurs. Because there is less resistance to dilational deformation once plastic yielding commences, it is to be expected that waves have less tendency to detach from a shock front than in a simple viscous model. This expectation is born out by numerical calculations (*figure 11*). Excepting this feature, along with details of symmetry and the magnitude of effective pressure, one-dimensional porosity waves that develop in a viscoplastic matrix are fundamentally similar to those in the simple viscous case [11].

7. Influence of thermally activated creep on viscous waves

It is well established [18] that shear viscosity (η) has an exponential dependence on temperature that can be expressed

$$\eta = \eta_0 \exp\left(-\frac{Q(1 - T/T_0)}{RT}\right) \tag{11}$$

where Q is the creep activation energy, η_0 is the viscosity at the reference temperature T_0. Alternatively, the variation in viscosity with depth due to the geothermal gradient from equation (11) is

$$\eta = \eta_0 \exp\left(-\frac{z - z_0}{l_\eta}\right) \tag{12}$$

where l_η is the 'e-fold length', the length scale over which there is an e-fold decrease (where e is the base of the natural logarithm) in shear viscosity with depth in the lithosphere, and z_0 is the depth at which the visco-

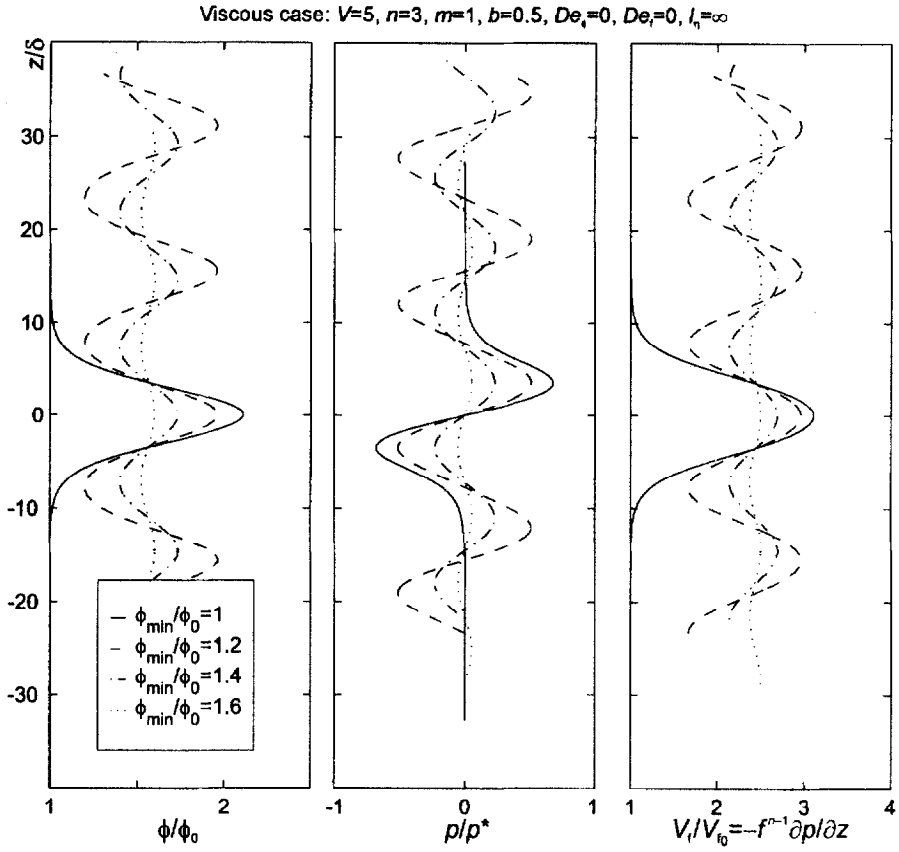

Figure 5. Analytic stationary solutions ($V = 5$, $n = 3$, $m = 1$, $De_\phi = 0$, $b = 0.5$, $De_f = 0$, $l_\eta = \infty$) for the porosity, pressure anomaly and fluid velocity distributions within solitary and periodic waves as a function of the background porosity (ϕ_{min}), relative to the background porosity necessary to obtain a solitary wave. Increasing ϕ_{min} is equivalent to reducing the excess volume (*figure 1*) carried by the waves. There is one solitary solution possible for a specified phase velocity, but there are an infinite number of periodic solutions. The periodic solutions are stable if either the excess volume or the obstructed fluid flux is relatively low.

sity is η_0. From equations (11) and (12) the e-fold length is

$$l_\eta = \frac{RT^2}{Q\frac{dT}{dz}} \tag{13}$$

The values of l_η for the rheologies and geothermal gradients characteristic of various regimes within the lithosphere are of the order of 200–5000 m (*figure 12*). This length scale is essentially identical to the typical viscous compaction lengths ($\delta \sim 100$–10000 m) cited in the context of constant shear viscosity models for melt extraction [22, 24]. Since both δ and the viscous compaction time scale t^* vary as $\sqrt{\eta}$ [equation (5)] it follows that constant viscosity models can only be valid on length scales of a few e-fold lengths and only if $\delta << l_\eta$.

The e-fold effect causes viscous porosity waves to become asymmetrical and slow to an essentially static state [11, 30]. Asymmetry arises because, for a given absolute effective pressure, the rocks at the base of the wave compact more rapidly than the rocks dilate at the wave front. The reduction in velocity is an intuitively clear consequence of strengthening, which must impede wave propagation. From one-dimensional models, Connolly [30] inferred that these effects would cause porosity waves to become sill-like as they propagated upward. Because one-dimensional waves are by definition planar, it is more convincing to demonstrate the stability of the one-dimensional wave in a two-dimensional model. For such a demonstration to be successful, it suffices to show that a circular wave, the stable form for an infinite e-fold length rheology [12, 14], spreads laterally as it rises. Accordingly, waves initiated by a sub-horizontal perturbation, such as might be created by a melting front, have a strong tendency to propagate as horizontal one-dimensional waves. Numerical solutions to equations (1) and (2) show that this is true (*figure 13a*). We conclude that for geologically plausible e-fold length scales, thermally activated viscous creep provides a strong stabilization of one-dimensional waves.

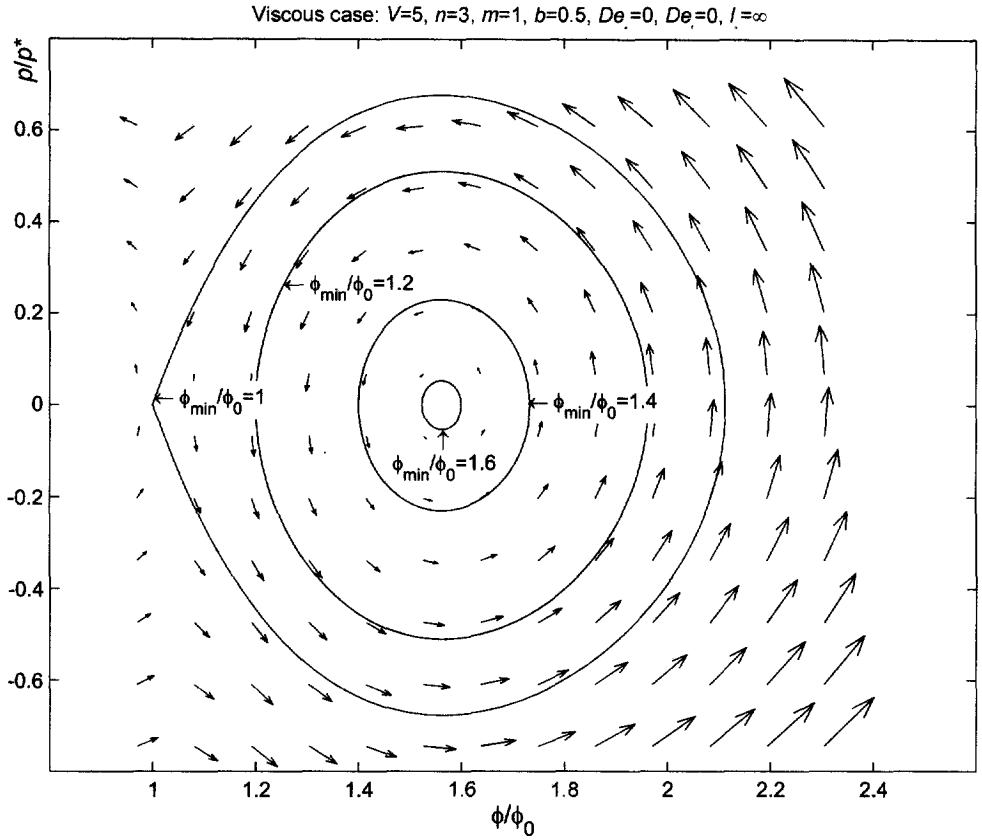

Figure 6. Pressure-porosity phase diagram for the wave solutions shown in *figure 5*. The characteristic of a solitary solution is that the gradients df/dz and dP/dz do not converge as the porosity and pressure decrease to the background levels. The trace of the solitary solution approaches ($P = 0, f = 1$) asymptotically, i.e. at infinite distance from the wave centre. There are no wave solutions outside of the region bounded by the solitary solution, solutions within the region are periodic (i.e. the trace of a solution closes on itself). The vectors indicate the gradients df/dz and dP/dz, these vectors must be tangential to the trace of stationary solutions.

Pressure gradients about a zero-dimensional perturbation are of comparable magnitude. Thus, if the strength of the matrix increases vertically on the scale of the compaction length, but does not vary laterally, then more deformation will occur in a lateral than in a vertical direction. For a two-dimensional wave, the process of lateral spreading is explained by the consideration that the lateral length scale of the waves is determined by the local viscous compaction length of the unperturbed matrix. This compaction length increases by an order of magnitude if a wave propagates vertically ~ $2.3l_\eta$. Thus, if a devolatilization or melting reaction occurs at a depth where $\delta = l_\eta/10$, i.e. where the e-fold effect is weak, two- or three-dimensional waves may nucleate from heterogeneities with a characteristic spacing of ~δ, but the waves must amalgamate to form a sill-like wave after propagating ~$2.3l_\eta$ (*figure 13b*). If $\delta << |l_\eta|$ the e-fold effect is weak and horizontal one-dimensional waves are unstable as has been demonstrated by linear stability analysis for constant shear viscosity [12]. Consequently, the vertical length scale of waves in an upward strengthening rheology must be ~ l_η. This logic implies that the aspect ratio (ε) of stationary two- and three-dimensional waves is [from equations (7) and (12)]

$$\varepsilon \approx 1 + \frac{\delta_0}{l_\eta} \exp\left(\frac{z - z_0}{2l_\eta}\right) \tag{14}$$

where δ_0 is the compaction length at depth z_0.

Equation (11) is a simplification in that viscosity is more plausibly related to the homologous temperature of the rock matrix rather than the absolute temperature [5]. This simplification is unimportant in the upper regions of the lithosphere, but with increasing depth the geotherm may become parallel to the mantle solidus in regions of asthenospheric melting. In such an environment the homologous temperature and matrix shear viscosity would be constant, and, at still greater depths steepening of the geotherm would lead to a decrease in the homologous temperature with depth. It follows that in this inverval, matrix shear viscosity increases with depth and the e-fold length must be negative. Equation

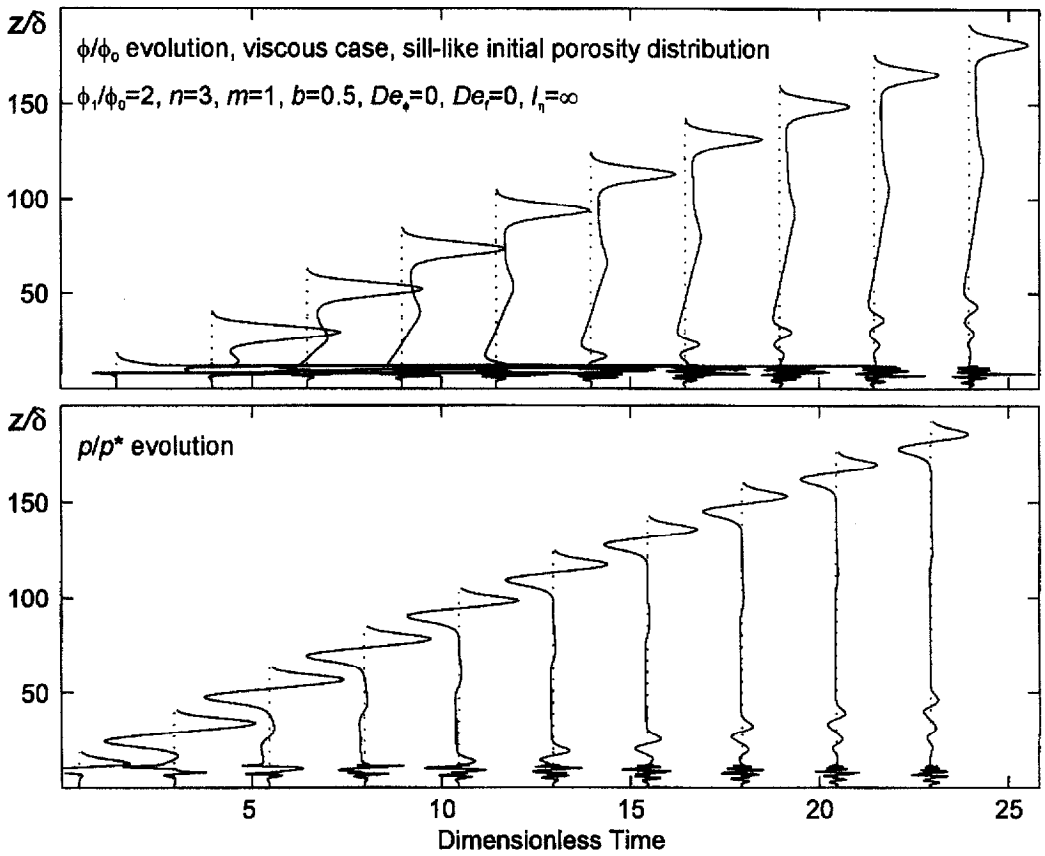

Figure 7. Transient depth ($-z$) profiles showing evolution of porosity and fluid pressure anomalies ($-p_e$) from a sill-like initial porosity distribution in a viscous matrix ($f_0 = 10$, $n = 3$, $m = 1$, $De_\phi = 0$, $b = 0.5$, $De_f = 0$, $l_\eta = \infty$). Profiles are scaled such that a unit dimensionless porosity (f) or dimensionless pressure is identical to a unit of dimensionless time. Initially, a large approximately solitary wave separates from the region of elevated porosity, by $t = 10$ transient periodic waves begin to propagate the residual excess volume. Wave velocity is proportional to amplitude [23], so with time the solitary wave distances itself from the periodic wave train.

(14), suggests the existence of two distinct regimes in this situation. If $\delta_0 < |l_\eta|$ the stable wave forms are prolate ellipsoids with an aspect ratio that becomes infinite as $\delta_0 / |l_\eta| \rightarrow -1$, in which case the waves become tube-like channels. The channelling behaviour differs from that observed in reactive transport models [15] in that the channels are stable and that the vertical extent of the channels is limited by the upward reduction of the viscous compaction length. An intriguing possibility related to this behaviour is that instabilities in a negative l_η-rheology may develop into self-propagating cracks [33, 34]. The second regime for a negative e-fold length rheology occurs when $\delta_0 > |l_\eta|$ in which case the aspect ratio from equation (14) is negative and there are no stable waves, i.e. fluid flow is dispersed. Variation in the e-fold length with depth thus provides an explanation for both the concentration of asthenospheric melts into vertical channels and the subsequent ponding of these melts in sills above the asthenosphere. In this context it is pertinent to observe that viscoplastic yielding also induces channelled flow, a subject that we do not explore further here.

8. Porosity shocks in the elastic limit

Porosity waves in an elastic matrix have received less attention than waves in a viscous matrix. Rice ([1], see also reference [35]) derived the stationary solution for the propagation of a stationary step-like shock into a flow obstruction for boundary conditions of constant flux and effective pressure. Conservation of mass requires that the shock propagates with a velocity given by equation (9); if the flux within the obstruction is small (i.e. $q_0 << q_1$), this velocity is approximately the particle velocity of the fluid beneath the obstruction

$$v_f = \frac{k\phi_1^{n-1}\Delta\rho g}{\mu} \tag{15}$$

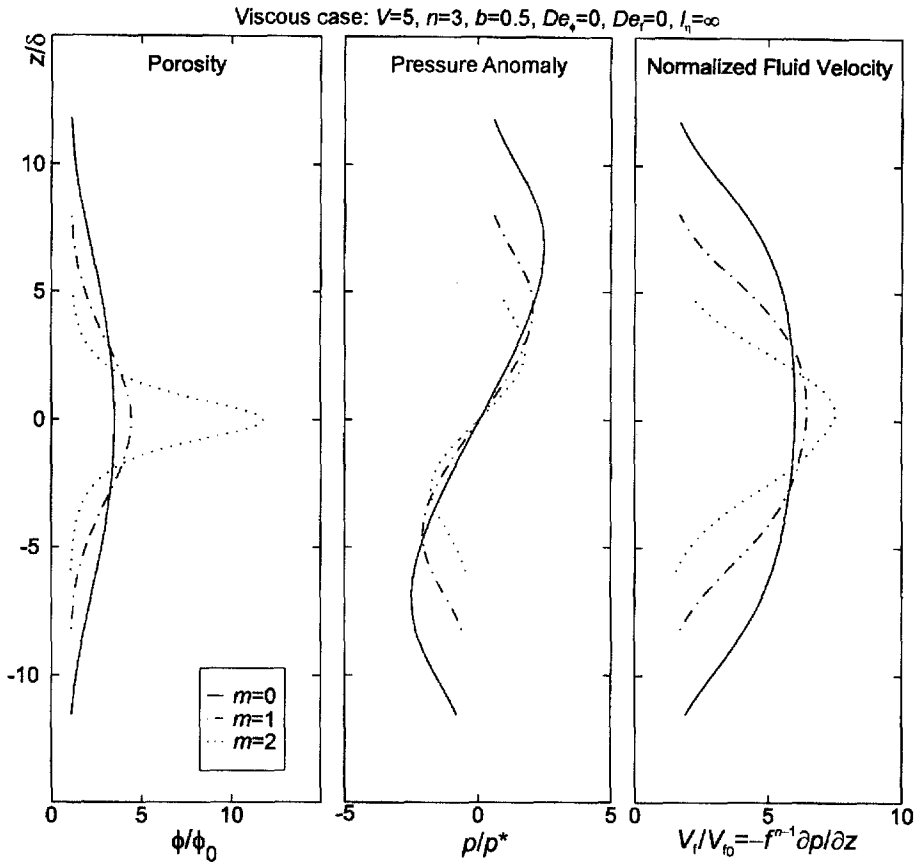

Figure 8. Stationary analytic solutions for the porosity, pressure anomaly and fluid velocity distributions for solitary waves (V = 5, n = 3, De_ϕ = 0, b = 0.5, De_f = 0, l_η = ∞) as a function of the rheological (bulk viscosity) porosity exponent m. Increasing non-linearity sharpens the transition between the wave and background porosity. For m = 1, in the limit of large porosity waves, the porosity distribution is approximately Gaussian [equation (10)].

In an elastic medium, permeability and porosity are functions of effective pressure. Equation (1) can thus be arranged to express a lower bound for the fluid pressure perturbation necessary to initiate the shock

$$\delta p_f \approx \frac{\ln(\phi_1)}{\beta_\phi} \quad (b = 1) \tag{16}$$

where ϕ_1 is the porosity beneath the obstruction. The essential difference with the viscous model is that in an elastic matrix fluid, pressure cannot decrease below its initial value if there is a constant fluid flux beneath the obstruction. Elastic shocks therefore cannot detach from their source [35]. Consequently, there are no solitary wave solutions of the compaction equations for an elastic matrix.

The initiation and propagation of an elastic shock from a step-like porosity distribution, and the initial conditions discussed earlier for the viscous case, are illustrated in *figure 1*. The presence of the obstruction causes fluid pressure and porosity to increase and fluid diffuses into the obstruction (*figure 1b*). When the increase in fluid pressure approaches a critical value, greater than that given by equation (16), elastic deformation becomes adequate to accommodate the fluid flux, pressure ceases to rise, and a stationary shock wave nucleates and propagates the obstruction upward with a velocity given by equation (9). If the initial porosity distribution is sill-like and fluid pressure rises to values for shock nucleation, the shock must change shape as it propagates to conserve the fluid mass. In this case, the shock is self-similar rather than stationary [35] and its amplitude and velocity fall asymptotically to those of the background porosity and fluid velocity. Although we have considered initial conditions of constant (zero) effective pressure, this is not a requirement for shock initiation. Indeed, because elastic deformation is incremental, shocks can propagate by elastic dilation at any effective pressure.

9. Viscoelastic fluid–rock interaction

Elastic behavior in compaction driven flow may arise from either, or both, fluid and matrix (i.e. pore) elastic

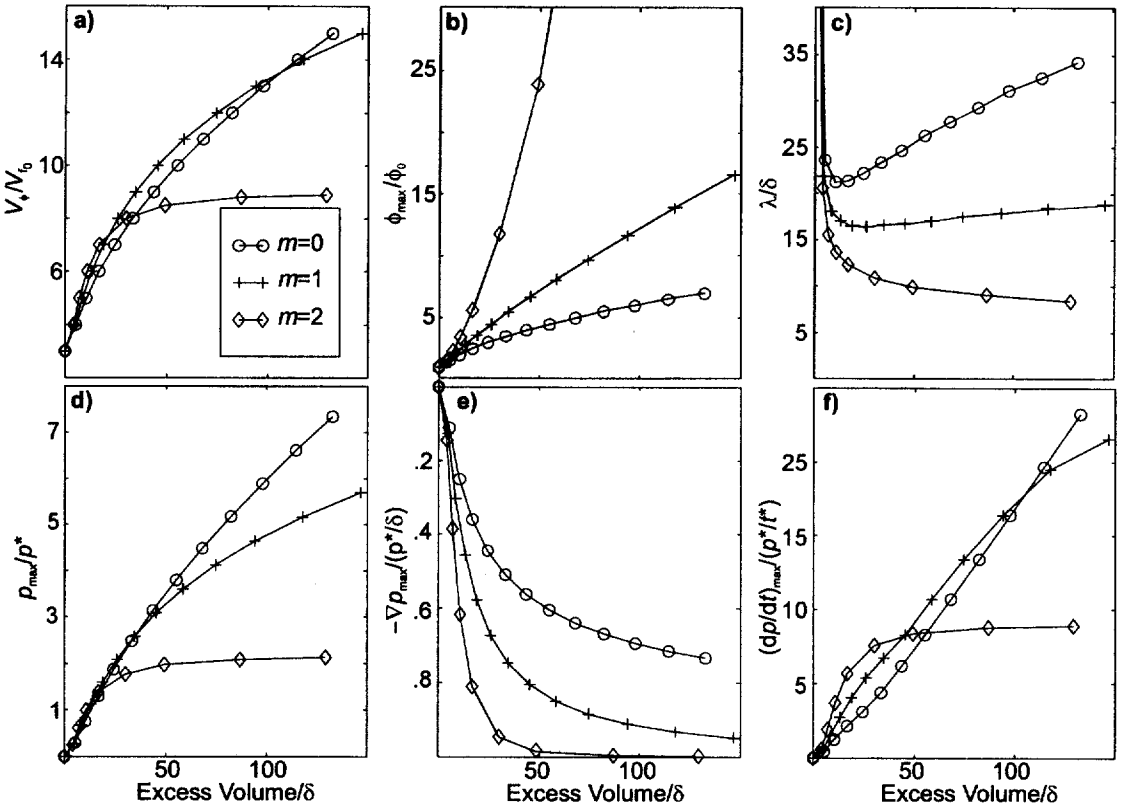

Figure 9. Properties of steady-state solitary porosity waves (V = 5, n = 3, De_ϕ = 0, b = 0.5, De_f = 0, $l_\eta = \infty$) as a function of the rheological porosity exponent m, and the excess volume carried by the waves. Increasing m potentially limits the efficiency of porosity waves as a transport mechanism since large values of m accelerate deformation with increasing porosity. Thus it becomes easier for the matrix to deform and in turn, the effective pressure gradients that drive hydraulic diffusion are reduced and the waves tend to grow into stagnant fluid segregations rather than propagate. Because the fluid pressure gradient diverges from the lithostatic gradient within porosity waves, large negative effective pressures may develop at the tip of a wave (see *d*). These pressures may induce plastic yielding. The dimensionless pressure gradient (see *e*) varies at the wave center varies form 0 to −1 (lithostatic to hydrostatic pressure gradients). The transient pressure variations (see *f*), which are strongest at the tail and tip of a viscous wave, that arise due to viscous deformation would magnify the role of elastic deformation in a viscoelastic matrix [i.e. in equation (1)].

compressibilities. The essential features of shock propagation in an elastic matrix are largely independent of fluid compressibility; this is not true in a viscoelastic matrix. In low temperature environments, pore compressibility may be the dominant source of elastic deformation and this justifies neglecting fluid compressibility. Alternatively, at high temperature, particularly in well-indurated rocks, fluid compressibility may dictate the elastic response of the system. We consider these extremes separately, before considering the most realistic scenario of compressible fluid and in a viscoelastic matrix.

9.1. Viscoelastic porosity shocks, incompressible fluid

The elastic character of a viscoelastic matrix is defined by the Deborah number, De_ϕ, which varies from zero in the viscous limit to infinity for the elastic limit [equation (8)]. Taking commonly accepted parameters relevant to mantle melt extraction and crustal devolatilization De_ϕ is ~ 10^{-4}–10^{-7}. Much larger effective Deborah numbers are appropriate if elastoplastic yielding occurs, as is to be expected in the case of porosity waves propagated by negative effective pressures. A point we return to in the next section.

For the step-like initial distribution, numerical solutions evolve rapidly to a stationary shock (*figures 14–16*). Thus the elastic mode of deformation appears to dominate the stationary solution for viscoelastic rheologies. Within viscoelastic shocks, viscous deformation produces a finite number of wave-like structures with amplitudes that diminish away from the shock front. For low De_ϕ, a sill-like porosity distribution evolves to produce transient shocks that mimic solitary and periodic stationary solutions. There are no solitary wave solutions for the flow obstruction amplitudes, porosity exponents, and viscous compaction length that we have

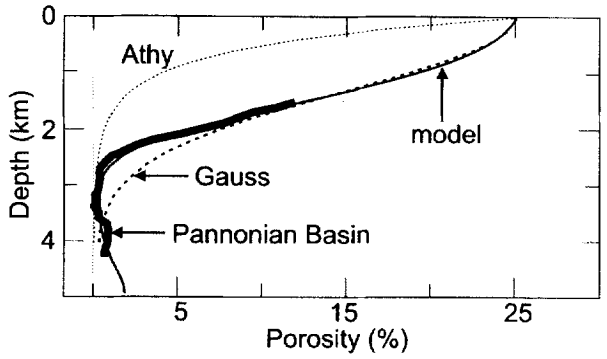

Figure 10. Comparison of the porosity–depth profile from marls in the Pannonian Basin (heavy solid curve) with the empirical Athy-exponential (thin dashed curve) and Gaussian (thick dashed curves) distributions, and the profile obtained by solving the viscous compaction equations for an 8 km thick sediment column with a water-filled initial porosity of 25 % with an initial permeability of 10^{-17} m^2 (thin solid curve). For the numerical calculation, $m = 1$, $n = 3$, the matrix shear viscosity is 10^{22} at 3 km depth, and $l_\eta \sim 1$ km [11]. The model profile is essentially stationary 30 My after the onset of compaction, the shape of the profile is insensitive to sedimentation rate and initial sediment permeability. The Pannonian Basin porosity (data from Szalay [41] as cited by Van Balen and Cloetingh [27]) values have been lowered by 2.5 %. The increase in porosity with depth in the lower portion of the Pannonian Basin is attributed to overpressure-induced secondary porosity. The Athy ($\phi = \phi_0 (\phi_{min}/\phi_0)^{z/\lambda}$) and Gaussian ($\phi = \phi_{min} + (\phi_0 - \phi_{min})\ 16^{-z^2/\lambda^2}$) porosity distributions are computed for $\phi_{min} = 0.001$, $\phi_0 = 0.25$, and $\lambda = 3000$ m. Large amplitude porosity waves are represented well by a Gaussian distribution in the limit of constant shear viscosity, which provides a sensibly better fit to the compaction front than the Athy model.

examined in this case. Aside from destabilizing the periodic and solitary wave solutions to the compaction equations, viscoelasticity dampens the waves, or wave-like structures in transient solutions, as compared to those that develop in the analogous viscous models.

9.1.1. Thermally activated creep

The temperature dependence of elastic parameters is weak in comparison to the Arrhenius dependence of viscous creep [5]. Consequently the primary controlling factor (physical heterogeneity excepted) on the evolution of deformation-propagated fluid flow through a matrix with a thermal gradient is the e-fold length for viscous deformation. If a thermal gradient exists in an otherwise uniform matrix, the matrix cannot be characterized by a single De_ϕ value, and the local Deborah number, from equations (7), (8) and (13), is an exponentially decreasing function of depth

$$De_{local} = De_0 \exp\left(\frac{z_0 - z}{2l_\eta}\right) \qquad (17)$$

where De_0 is De_ϕ at z_0 and l_η is assumed to be constant. The implication of this temperature dependence is that the dominant mode of deformation will be increasingly elastic toward the surface. Thus, essentially viscous shocks or waves at depth may undergo an abrupt transition into an elastic shock. The transition may be dramatic because the relatively slow, large amplitude viscous waves, are transformed into low amplitude, high velocity, elastic shocks (*figure 17*). Moreover, the periodicity of the viscous waves is inherited by the elastic shocks with the result that flow in the elastic regime may be markedly episodic. Although the character of viscous flow is primarily one-dimensional, lateral porosity heterogeneities can be preserved almost indefinitely. In two-dimensional models, the elastic shocks nucleate preferentially from these heterogeneities and this may cause lateral focusing of the fluid from the viscous shock into a plume shaped elastic shock (*figure 17c*). Thus, transient fluid flow patterns in a viscoelastic matrix vary strongly both in space and time.

9.2. Viscoelastic porosity shocks, incompressible matrix: negative shocks

Flow of a slightly compressible fluid in a viscous matrix is characterized by the fluid Deborah number, De_f, which varies from zero to infinity between the limits of incompressible fluid flow in a viscous matrix and compressible flow in a rigid matrix. Elastic propagation of a shock front is impossible if $De_\phi = 0$, because there is no mechanism by which fluid compressibility can affect permeability. However, if the matrix porosity is underpressured, viscous compaction and elastic compression of the fluid act in concert and create a 'negative' shock, where by negative we mean that porosity increases in the direction of flow. The stationary solution for this shock is the antithesis of the solution for $De_\phi > 0$ and $De_f = 0$, in that shock separates a uniform background porosity from an overlying elevated porosity, and that the viscous wave-like structures that decay upward (*figures 18* and *19*). If De_f is vanishingly small, this solution becomes essentially indistinguishable from a periodic solution consisting of solitary waves (*figure 20*), a result obtained numerically [30].

The importance of the stationary solution for $De_\phi = 0$ and $De_f > 0$ is that it provides a mechanism by which the initial porosity of a steady, non-compacting system, can be recovered after a perturbation. Since the stationary solution for $De_\phi > 0$ and $De_f = 0$ can propagate such a perturbation into the initial porosity, the result that there are stationary solitary porosity wave solutions for compressible fluid flow in a viscoelastic matrix (i.e. $De_\phi > 0$ and $De_f > 0$) can be anticipated.

10. The zero porosity limit, viscoelastic porosity waves

The most important distinction between elastic and viscous matrix rheologies occurs in the limit of zero

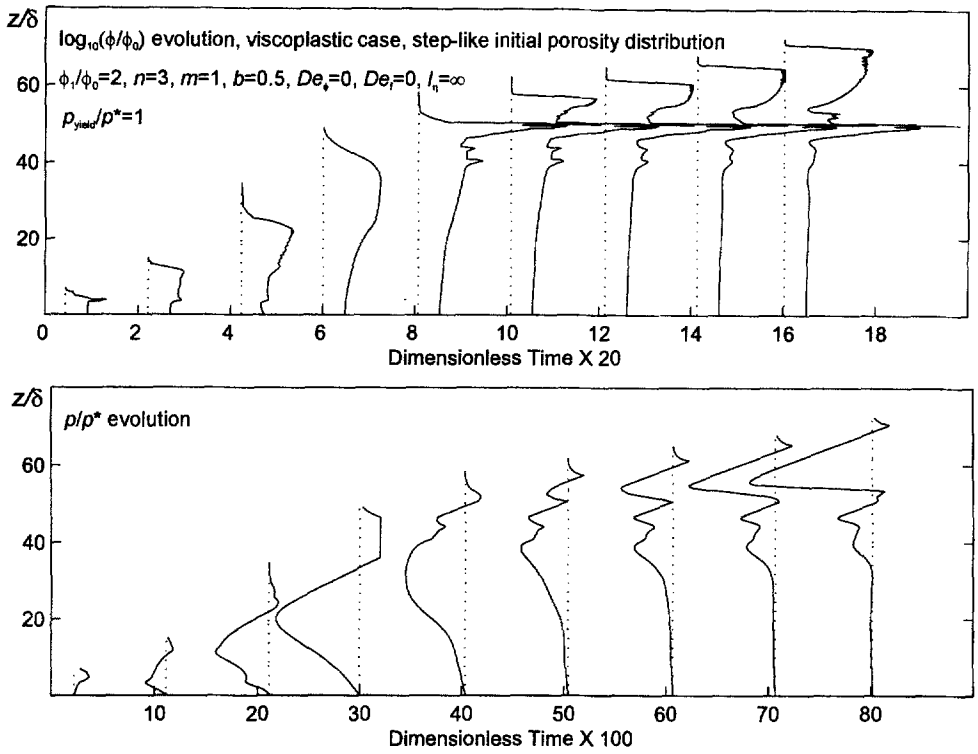

Figure 11. Transient depth ($-z$) profiles showing evolution of porosity and fluid pressure anomalies (i.e. $-p_e$) for $f_0 = 10$, sill-like initial porosity distribution in a viscoplastic matrix ($f_0 = 2$, $n = 3$, $m = 1$, $De_\phi = 0$, $b = 0.5$, $De_f = 0$, $l_n = \infty$) with plastic yielding at $p / p^* = 1$. Porosity profiles are scaled such that a log unit dimensionless porosity (f) corresponds to 20 units of dimensionless time, and 1 unit of dimensionless pressure is identical to 100 units of dimensionless time. The model demonstrates that, in contrast to the simple viscous case (*figures 3* and *4*), large negative effective pressures are not necessary to propagate shocks or solitary waves in a viscous matrix with plastic yielding. Plastic yielding does not otherwise change viscous wave propagation, which is fundamentally limited by the rate of viscous compaction (see also Connolly [11]).

hydraulic connectivity, an important limit for a variety of geologic processes. Barcilon and Richter's [23] stationary solution for solitary waves gives vanishing velocity and requires infinite fluid pressure and wave amplitude (i.e. $\phi = 1$) for zero background porosity. Thus, there are no solitary waves in an idealized viscous matrix in this limit. This implies that solitary waves propagating through a viscous matrix with finite background porosity would be trapped beneath a region of zero porosity. This process must lead to increasingly strong gradients in both porosity and pressure, as implied by Barcilon and Richter's [23] solution. However, transient steepening of the pressure gradient produces an inexorable magnification of the importance of the elastic deformation mode in equation (1), raising the local Deborah number near the flow obstruction. In contrast to fluid flow in a viscous matrix, there is no singularity at zero porosity in Rice's [1] stationary solution for the propagation of a shock through an elastic matrix. Transient solutions for the development of such a shock are also well established [21]. The physical basis for these solutions is that the effective pressure gradient at the shock front is infinite, and thus hydraulic diffusion can drive fluid flow into the zero porosity matrix by exploiting flaws. Because of the infinite effective pressure gradient, shock propagation is not limited by processes at the shock front, but rather by the rate at which fluid is supplied to the front by compaction processes at greater depth. In this respect, the propagation is analogous to viscoplastic wave propagation.

The two distinct stationary solutions obtained for fluid flow in a viscoelastic matrix with incompressible fluid and for a compressible fluid in a viscous matrix, show that elasticity plays different roles in equations (1) and (2). Fluid compressibility is not present in equation (1) and therefore cannot influence the hydraulic properties of the matrix. Consequently, the primary effect of fluid compressibility is antithetic to viscous compaction in that it raises fluid pressure in response to compaction. Hence, the stationary solution for $De_\phi = 0$ and $De_f > 0$ in which fluid pressure varies inversely with porosity at the shock front (*figures 18* and *19*). In contrast, poro-elasticity enters both equations (1) and (2), but in the elastic limit applicable at a shock front, equa-

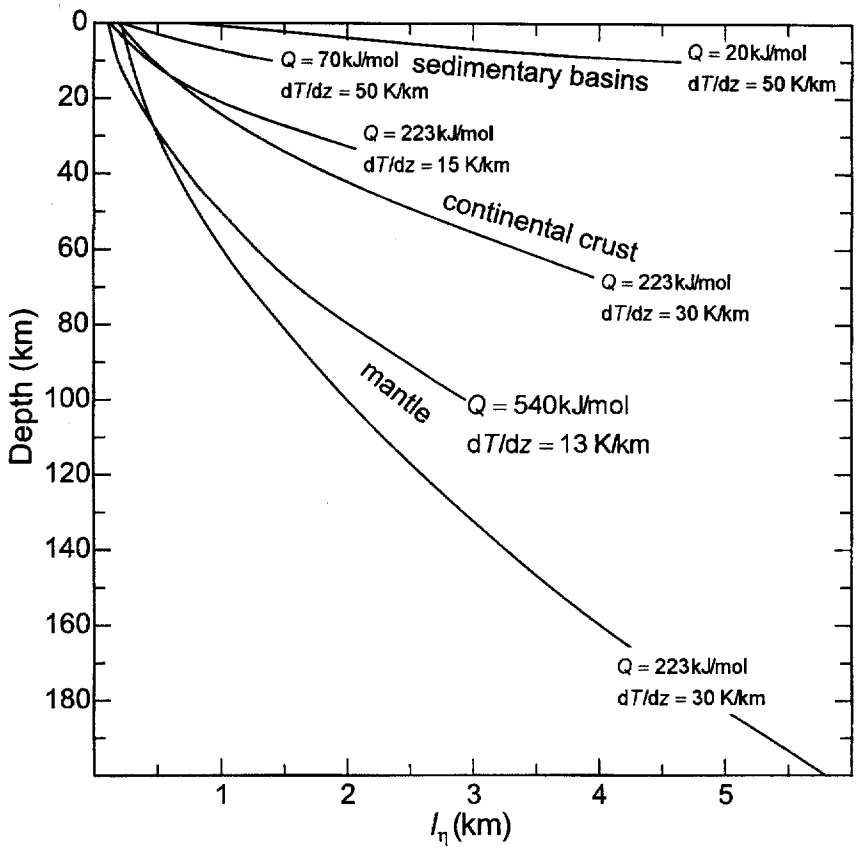

Figure 12. Typical e-fold lengths, l_η, for viscous deformation in lithospheric environments as function of depth. The e-fold length [equation (13)] is the length-scale over which viscosity is reduced by a factor of e with depth in the lithosphere due to the geothermal gradient and the thermal activation energy of viscous deformation. All calculations are for a surface temperature of 273 K and constant geothermal gradients. For sedimentary basins, l_η is for a rheology dominated by pressure solution creep of quartz (Q = 20-70 kJ·mol^{-1} [42]), and a geothermal gradient of 50 K·km^{-1} extrapolated to a depth of 10 km. For continental crust, l_η is for power-law creep of quartzites (Q = 223 kJ·mol^{-1} [43]) and geotherms of 15 and 30 K·km^{-1} extrapolated to a maximum temperature of 1273 K. For the earth's mantle, l_η is for power-law creep of olivine (Q = 540 kJ·mol^{-1} [18]) and geotherms of 6.5 and 13 K·km^{-1} extrapolated to a maximum temperature of 1573 K.

tion (1) requires that porosity is proportional to fluid pressure (*figures 15* and *16*). These relationships suggest that for the general case of $De_f > 0$ and $De_\phi > 0$, the possible stationary solutions must depend on the ratio De_f / De_ϕ, such that there is a transition from positive to negative shocks with increasing values of this ratio. The solution at this transition must be a solitary viscoelastic wave, but because this solution occurs for a unique value of De_f / De_ϕ it is of little interest. The transition is, however, of much greater significance in the limit of zero porosity because a negative stationary shock cannot exist in this limit. It follows that if solutions exist they must permit propagation of a solitary porosity wave through a matrix with no preexisting hydraulic connectivity. We obtain two stationary solutions for fluid flow in a zero-porosity viscoelastic matrix that supports this logic. For an incompressible fluid ($De_f / De_\phi = 0$), the stationary solution is a shock that may have wave-like structures developed behind a step-like front (*figure 21*). For a relatively compressible fluid ($De_f / De_\phi = 2$) the stationary solution is an asymmetric solitary porosity wave (*figure 22*). In contrast, to simple viscous solutions, which are solitary waves in both porosity and pressure, the pressure wave in this case is a negative shock. Thus, for finite background porosity the stationary solutions to the compaction equations are positive or negative shocks, whereas for zero porosity the solutions are either positive shocks, or a solitary porosity wave. The length scale for waves in the former case may be influenced by the background porosity. Thus, for waves produced by small ($\phi_1 \sim \phi_0$) and large ($\phi_1 >> \phi_0$) flow obstructions, the appropriate length scale varies, respectively, between the initial viscous compaction length above and below the flow obstruction. In either case, the compaction length may be influenced, if not determined by the e-fold effect, such that the waves may have sill- or

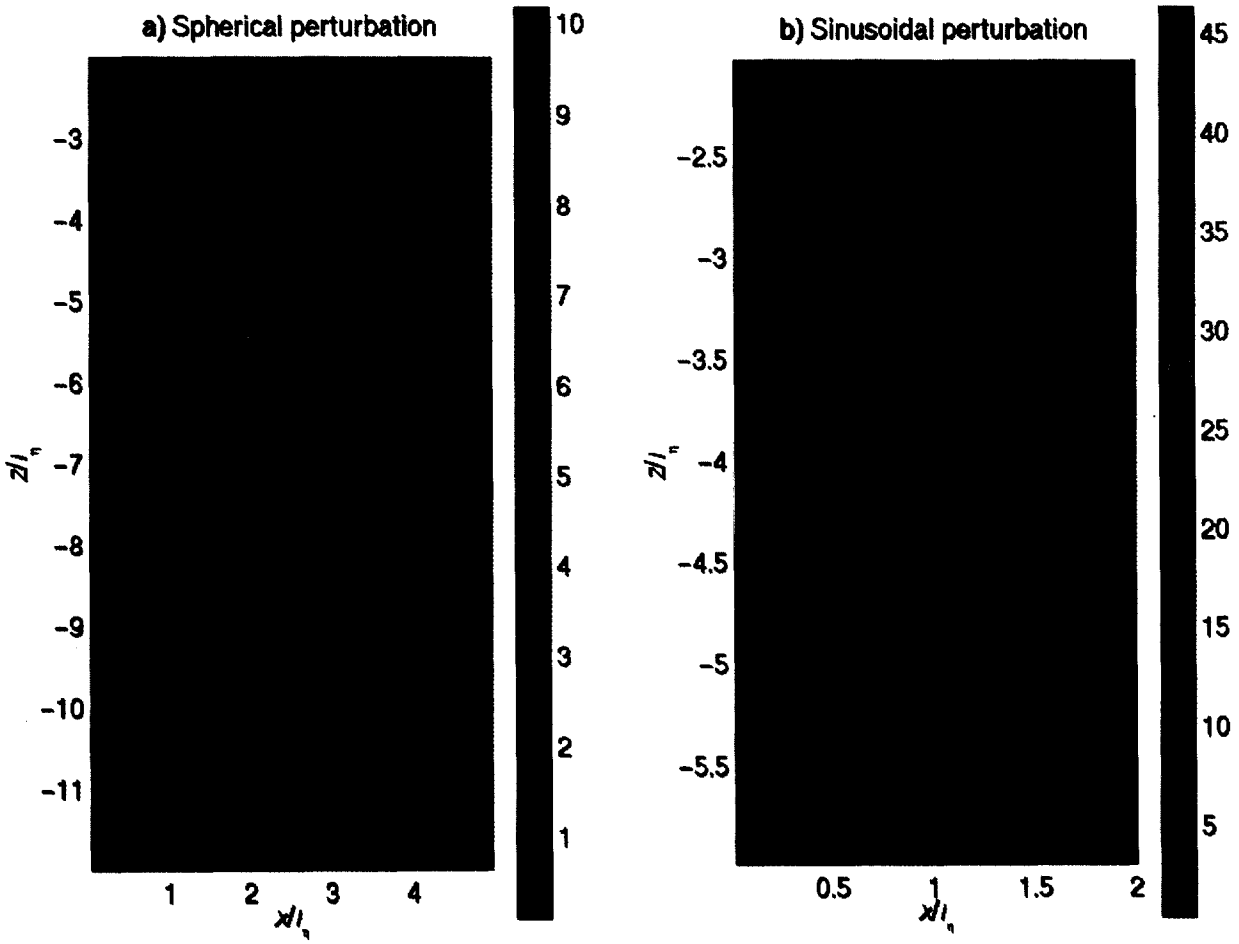

Figure 13. Transient two-dimensional porosity waves in an upward strengthening ($l_\eta > 0$) viscous matrix and slightly compressible fluid ($De_f = 3.8 \cdot 10^{-6}$). For both examples the local viscous compaction length, δ, in the unperturbed matrix is $0.1 l_\eta$ at the average depth of the initial perturbation. **a.** Waves (at $t = 22.5\ t^*$) initiated by a circular (sill-like) perturbation to the porosity with $\phi_1 / \phi_0 = 10$ and a radius of $l_\eta / 2$ centered at ($x/l_\eta = 0$, $z/l_\eta = -11$). **b.** Waves (at $t = 0.5\ t^*$) initiated by a sinusoidal (step-like) front, the trace of which is visible in the lower portion of the diagram, bounding a region of elevated initial porosity ($\phi_1/\phi_0 = 10$) at depth. Because the perturbations are placed at a depth at where $\delta < l_\eta$, the stable wave shapes are initially spherical as would be the case in a matrix of constant viscosity. As the waves propagate upward the local compaction length becomes comparable to l_η and the anisotropy of the matrix begins to influence the wave shapes. For the spherical perturbation, this causes the wave to flatten to an oblate ellipsoid with an aspect ratio that is an exponential function of depth [equation (14)]. The initial wave leaves a region of low porosity in its wake; this lowers the local compaction length and therefore reduces the importance of the e-fold effect for subsequent waves. For the sinusoidal perturbation lateral spreading stabilizes a one-dimensional sill-like wave from the spherical waves generated at the perturbation after propagation of $\sim 2 l_\eta$. These results imply that if $\delta \geq l_\eta$ fluid flow occurs by horizontal waves unless there are horizontal heterogeneities on a lateral distance scale substantially greater than the local viscous compaction length. Upward strengthening results in an exponential increase in the compaction time-scale with decreasing depth [equations (8) and (13)], which results in progressive slowing of the waves. If the e-fold effect is reversed ($l_\eta < 0$), the dike-like waves are stabilized.

dike-like geometries depending on the thermal environment.

11. Viscoelastoplastic matrix: large De_ϕ

The matrix Deborah number is essentially a function of δ and β_ϕ [equation (8)]. As characteristic values of the bulk modulus ($1/\beta_\phi$) for indurated rocks in compression are $\sim 10^9$ Pa [5], large values of De_ϕ imply extraordinary values of δ, and therefore that the length scale of stationary viscoelastic waves discussed previously is implausibly large (~1000 km). This problem is resolved if the importance of plastic yielding is recognized, since the tangential bulk modulus of an elastoplastic rock in tension, the modulus relevant for wave propagation,

Fig13 Connolly&Podladchikov

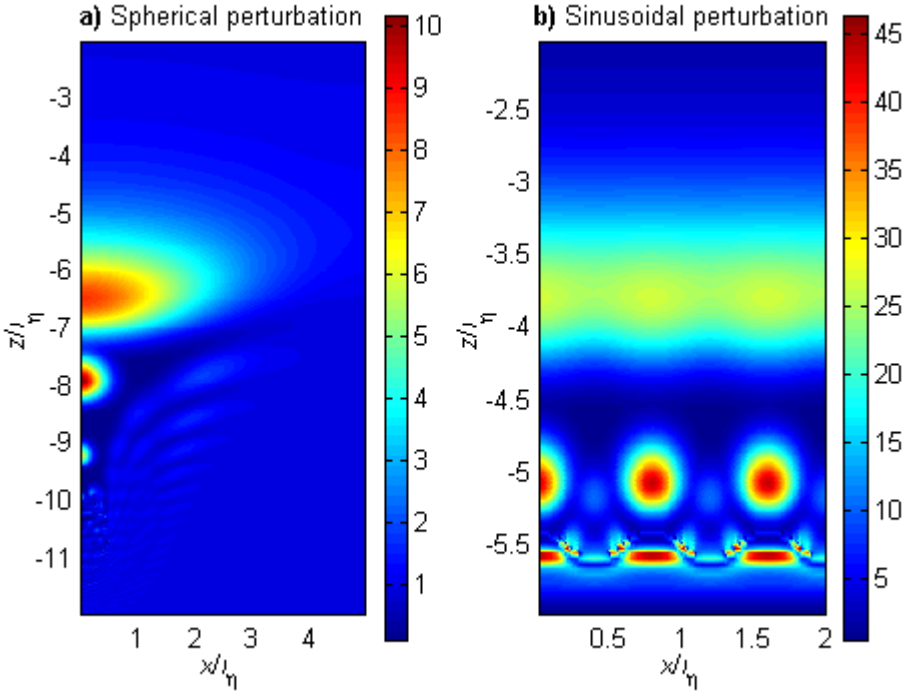

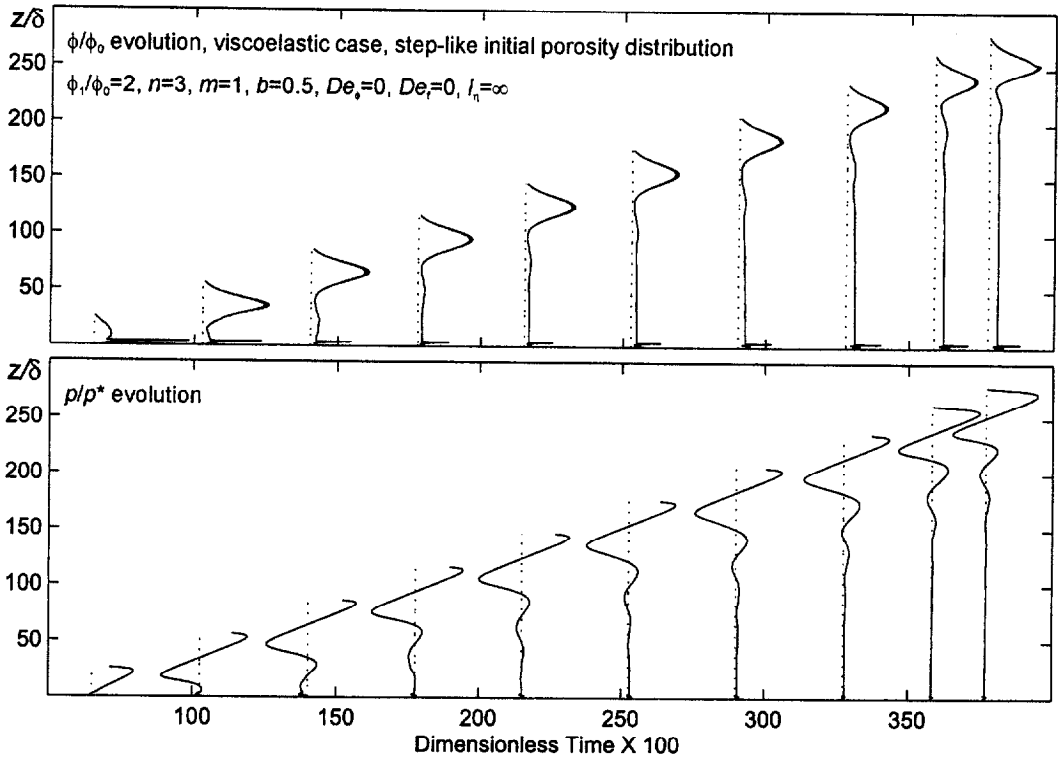

Figure 14. Transient depth (−z) profiles showing evolution of porosity and fluid pressure anomalies ($-p_c$) for a sill-like initial porosity distribution in a viscoelastic matrix with an incompressible fluid ($f_0 = 10$, $n = 3$, $m = 1$, $De_\phi = 0$, $b = 0.5$, $De_f = 0$, $l_\eta = \infty$). Profiles are scaled such that a unit dimensionless porosity (f) or dimensionless pressure is identical to 200 units of dimensionless time. The transient solution anticipates the stationary wave solution for a viscoelastic matrix, which is a shock connecting to distinct levels of porosity. The wave-like structures developed within the shock reflect the viscous deformation mode of the matrix. In contrast to the viscous case (*figure 4*), the viscoelastic shock does not grow indefinitely with time and therefore it must propagate with a velocity given by equation (9), which is greater than the velocity of the viscous shock.

varies from the value of the modulus in compression to infinity for ideal tensile failure [36]. In principle, incorporation of elastoplasticity requires Deborah numbers corresponding to the two moduli. However, in geological environments where viscous deformation is significant, elastoplastic deformation of the matrix is only important for the propagation of a wave front, in which case the bulk modulus in tension is appropriate. Thus viscoelastoplasticity does not fundamentally alter the character of wave propagation from the viscoelastic case, but it does increase the values of the De_ϕ appropriate for natural processes, thereby reducing the length scale of the waves. The same argument cannot be developed for propagation of the tail of a travelling wave in a viscoelastic matrix because the tail is propagated by compression and controlled largely by De_f. Thus, the propagation of porosity waves in natural viscoelastoplastic environments can be described as a special case of viscoelasticity characterized by $De_\phi >> De_f$. Waves that develop in this case are highly asymmetric and tend toward the limit represented by flow of an incompressible fluid in a viscoelastic matrix (*figure 21*).

12. Summary and discussion

Porosity waves are a mechanism by which fluid flow can be accomplished at substantially different rates than predicted by classical Darcyian models. The essential conditions for the initiation of waves is that permeability is an increasing function of porosity. Under these conditions an obstruction to compaction driven flow can sharpen and propagate as a shock. Disregarding dissipative effects that may arise from pre-existing spatial variation in the matrix properties, the shock may evolve to a stationary state, in which case the shock propagates with a constant velocity that is less than or equal to the Darcyian velocity of the fluid behind the shock. Alternatively, the shock may either slow and compress or become increasingly attenuated and decompose into waves with phase velocities that are greater than the initial velocity of the fluid. The former case is a potential

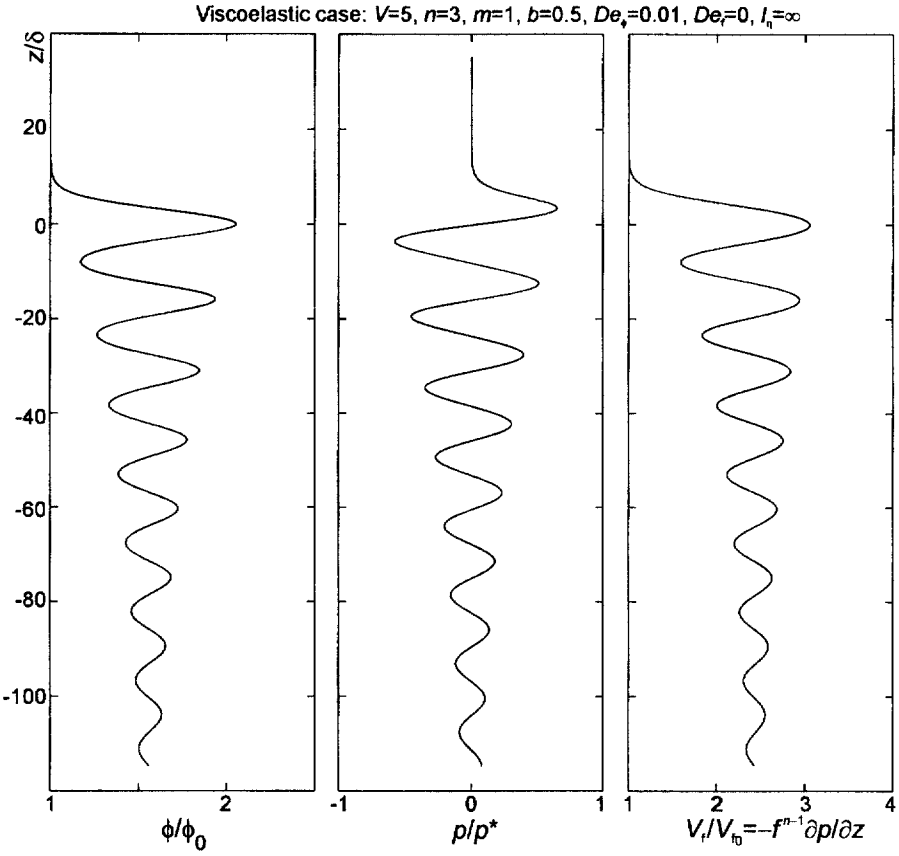

Figure 15. Analytic stationary solution for a shock developed by flow of an incompressible fluid in a viscoelastic matrix ($V = 5$, $n = 3$, $De_\phi = 0.01$, $b = 0.5$, $De_f = 0$, $l_\eta = \infty$). Stationary shock solutions are possible in an elastic matrix, but are unknown for the viscous case. The solution here suggests that solitary waves are not possible for flow of an incompressible fluid in a matrix with finite elastic character.

mechanism of forming fluid compartments during sediment compaction, whereas the latter is of interest in the context of melt extraction. The geological literature on this subject has been largely concerned with melt extraction, and in particular, the exploration of a viscous model of compaction in which the matrix viscosity is constant. Such a model is useful for understanding some features of compaction, but it is inconsistent with both theoretical and experimental knowledge of natural rheology. Here we have developed a more complete model that eliminates many of these inconsistencies. Our model takes into account the dependence of bulk viscosity on temperature and porosity, as well as the existence of elastic and plastic modes of deformation. In general, plastic deformation can be treated as a special case of elastic or viscous deformation. The exception to this generality is the limit ideal plasticity at zero effective pressure, in which case wave propagation is impossible.

12.1 Wave classification

The stationary solutions to the compaction equations dictate the transient evolution of shocks that develop in response to a flow obstruction. For pure viscous and viscoplastic limiting behavior, we find both periodic and solitary wave stationary solutions. The transition between the solutions depends on the magnitude of the excess volume carried by the wave and the Darcyian velocity of the background fluid flux. Periodic solutions are possible for all velocities, whereas solitary solutions require large volumes and low velocities. In a viscous matrix with vanishing hydraulic connectivity, the pressure required to propagate the waves with vanishingly small velocities becomes infinite. The application of pure viscous rheological models to problems concerning the extraction of mantle melts is therefore questionable. Dilational deformation in a viscous matrix, the mechanism of wave propagation, requires negative effective

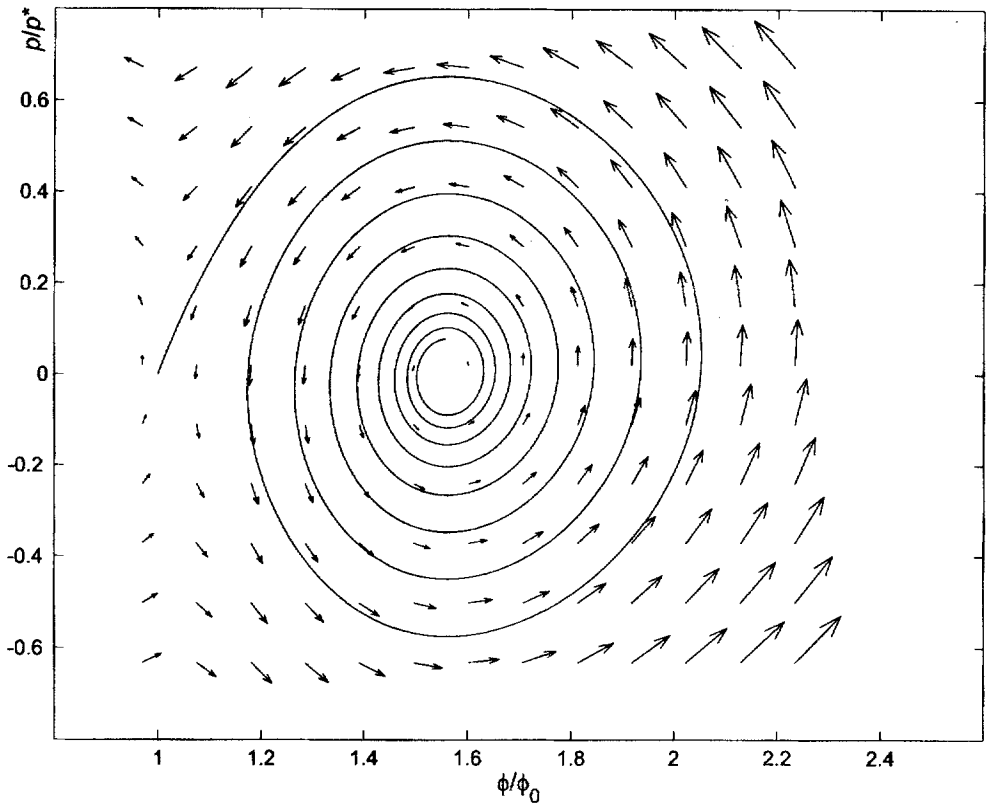

Figure 16. Pressure–porosity phase diagram for the stationary viscoelastic shock solution shown in *figure 15*. The spiral trace of the solution shows that the effect of elasticity is to dampen the periodic and solitary solutions possible in a viscous matrix (*figure 6*). Because the trace begins in a clockwise direction from the background porosity the wave-like structures within the shock converge to the elevated porosity beneath the shock front.

pressures that may be unsustainable because of plastic yielding (e.g. hydrofracture). However, the essential features of wave propagation in a viscoplastic matrix are unchanged from a simple viscous model because wave propagation becomes limited by the rate at which viscous compaction drives fluid to the uppermost region of a wave. In an elastic matrix, there are no stationary wave solutions to the compaction equations, but there are stationary solutions for porosity shocks that propagate with a velocity that is less than or equal to the velocity of the fluid behind the shock [1, 35]. In contrast to viscous or viscoplastic waves, elastic shocks do not require negative effective pressures for propagation and can propagate into a matrix with no connected porosity. The latter property is requisite for relevance to geological processes, and suggests that a viscoelastic model rheology has a wide range of potential geological applications. Flow of a slightly compressible fluid in a viscoelastic rheology is characterized by two dimensionless parameters, in addition to those conventionally used to describe compaction driven flow in a viscous matrix: (1) De_f, the fluid Deborah number, which varies from zero to infinity between the limits of incompressible fluid flow in a viscous matrix and compressible flow in a rigid matrix; and (2) the matrix Deborah number, De_ϕ, which varies from zero to infinity between viscous and elastic limiting behavior. Stationary solutions for viscoelastic rheologies and an incompressible fluid consist of a shock front similar to a pure elastic shock with one or more wave-like structures of diminishing amplitude developed behind the front. The most interesting, and geologically significant, stationary solutions are for flow of a slightly compressible fluid in a viscoelastic matrix with no connected porosity. The solutions in this case are in general shocks, but a solitary porosity wave solution is also possible. For a matrix with significant viscous character, viscoelastic shock solutions consist of a step-like front that rises from the background porosity, ϕ_0, with one or more large amplitude wave-like structures behind the front. The wave-like structures decay to a new level of porosity at $\phi_1 > \phi_0$, which may be orders of magnitude less than the maximum ampli-

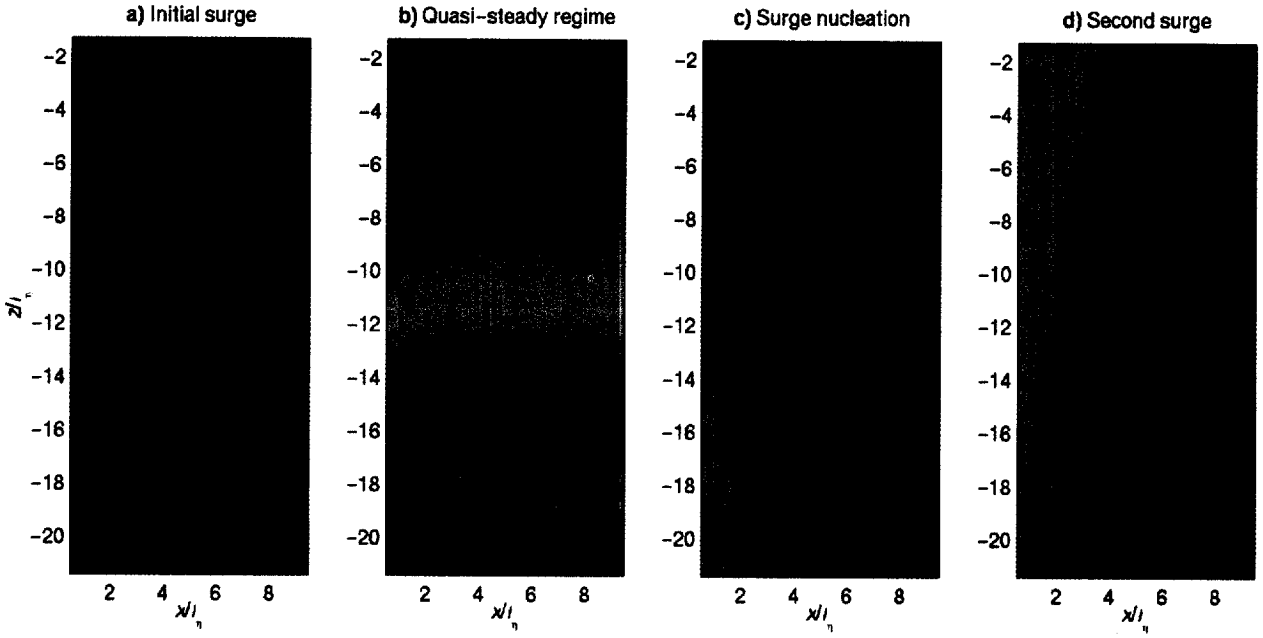

Figure 17. Transient porosity waves in an upward strengthening ($l_\eta > 0$) viscoelastic matrix (characterized by the local values $\delta = l_\eta/4$, $De_\phi = 0.017$, $De_f = 3.8 \cdot 10^{-6}$ at $z = 20\ l_\eta$, with $m = 1$, $n = 3$ and $b = 1$). The waves are initiated by a sill-like horizontal region with dimensionless porosity $f = 20$ and a vertical extent of $l_\eta / 4$, two-dimensional instability is induced by raising the porosity in this region by 20 % for $x = 0 - l_\eta/4$. **a.** $t = 0.001$, the initial porosity distribution is largely intact, but an elastic pressure surge has propagated $10 l_\eta$ from the elevated domain of porosity. **b.** $t = 0.734$, in the upper half of the model region, the porosity has formed a smooth shock-like structure, characteristic of elastic deformation, that continuously drains the fluid from the initial perturbation. Below the perturbation, viscous deformation has generated essentially one-dimensional viscous wave-like structures. A relict of the original lateral heterogeneity is preserved as a region of low porosity at $x = 0$. Because this region has lower pore compressibility, it serves as a point of nucleation for the pressure surge (see *c*) ($t = 0.777$) that occurs when a viscous wave increases the rate of fluid flow into the elastic region. The viscoelastic character of the surge is manifest by fainter wave-like structures developed within it. The surge reaches the surface by $t = 0.778$ (see *d*), and the fluid distribution is restored to a condition similar to that in *b* at $t = 0.820$. The model illustrates the extreme variation in time scales of fluid flow due to the e-fold effect. To put the dimensionless numbers in perspective, taking plausible parameters for a metamorphic environment ($l_\eta = 1$ km, $\eta_0 = 10^{20}$ Pa·s, $k = 10^{-22}\text{m}^2$, $\mu = 10^{-4}$ Pa·s, $\Delta\rho = 2000$ kg·m^{-3}, and $\phi_0 = 0.1$ %), the surge velocities are ~0.4 m·y^{-1}, whereas the viscous dominated wave propagation at depth occurs at ~$4 \cdot 10^{-3}$ m·y^{-1}. Moreover, after the initial pressure surge, conditions in the 'upper crust' remain approximately steady for ~$4 \cdot 10^6$ y before the nucleation of the second surge. The system then recovers to a state similar to that illustrated in *b* after $2 \cdot 10^5$ y. The colour-scales are chosen so that blue corresponds to $f = 0.1$, and red corresponds to the maximum porosity in each diagram: $f_{max} = 42$ (see *a*), $f_{max} = 4.5$ (see *b*), $f_{max} = 72$ (see *c*), and $f_{max} = 50$ (see *d*).

tude of the shock structures. In this respect, the shocks may resemble viscous solitary waves. The shock tip is propagated by elastic deformation, and propagation is limited by the rate at which viscous compaction drives fluid to the shock front.

12.2. Zero porosity limit

In compaction models of melt extraction it has been generally assumed that the mantle rocks through which melt migrates have a finite viscous compaction length. This assumption can only be justified by tortuous logic, because it implies that there is a melt-filled porosity in the mantle prior to melt extraction. If this assumption is discarded, and mantle melting is presumed to occur in such a way as to create an interconnected melt-filled porosity bounded by rocks with no melt, i.e. zero porosity, then viscous compaction within the melt-filled region will generate strong variations in pressure near the impermeable barrier. These variations raise the local matrix Deborah number, so that despite low De_ϕ values characteristic of the mantle, the deformation at the melt front is essentially elastic in character. The melt is then transported into the zero-porosity matrix by an elastic shock, which may be followed by a large wave-like structure. If the melt is relatively incompressible ($De_f < De_\phi$), the shock must remain attached to the source rocks. If a process such as freezing causes detachment of the shock, the wave will decay leaving a trail of melt in its wake. In contrast, if the melt is relatively compressible, the wave can detach from its source without

Fig17 Connolly&Podladchikov

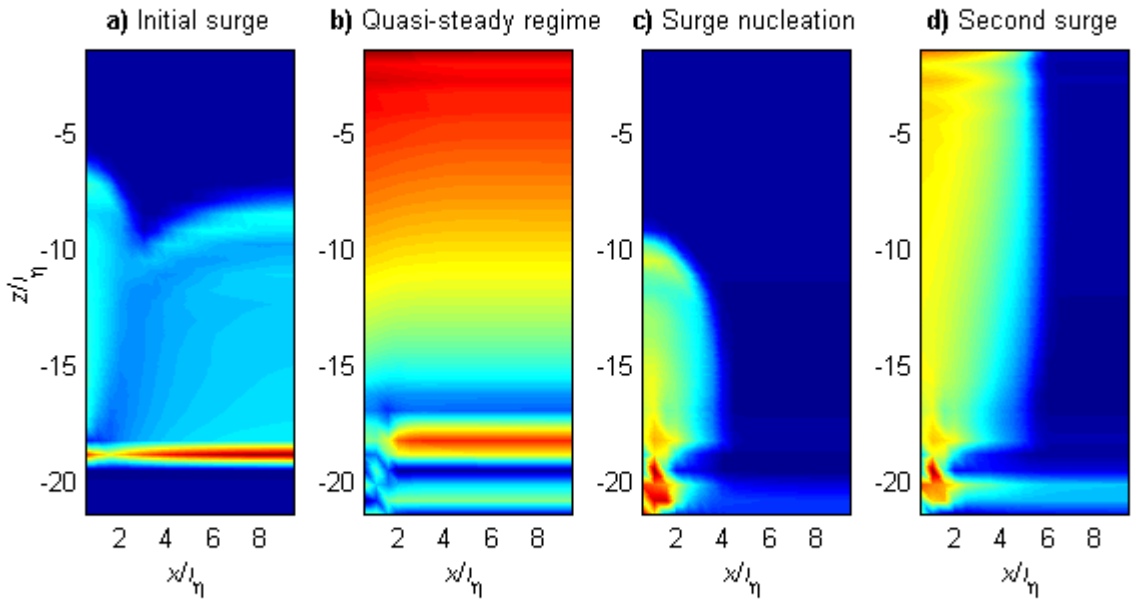

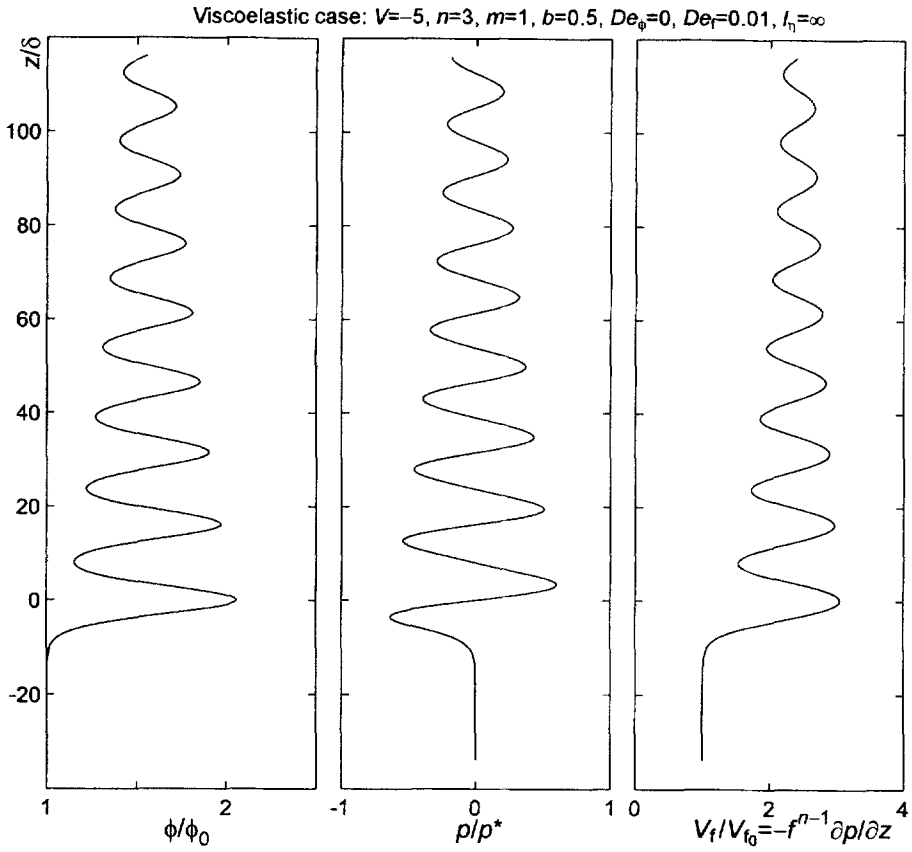

Figure 18. Analytic stationary solution for a 'negative' shock developed by flow of a compressible fluid in a viscous matrix ($V = -5$, $n = 3$, $De_\phi = 0$, $b = 0.5$, $De_f = 0.01$, $l_\eta = \infty$). The stationary shock solution for this case is peculiar in that porosity changes from the background level to establish a new elevated level of porosity above the shock. This suggests that fluid compressibility can act to damp the wave-like structures that form behind a shock in a viscoelastic matrix and restore the porosity to the background level. The shock propagates downward, against the direction of fluid flow.

decaying. A similar process can be envisioned for the transport of metamorphic or diagenetic fluids through rocks in which an interconnected porosity is texturally unstable. There has been much discussion of the limited capacity of porosity waves as a mechanism for transporting geochemical signatures. The nature of this limitation is a consequence of the fallacious assumption that geologic fluid transport invariably occurs in the presence of a background fluid flux, which implies that the fluid within the waves must be diluted continuously with propagation. This is not the case for wave propagation in a matrix with no initial hydraulic connectivity, since the wave and fluid travel with the same velocity. Nonetheless, the chemical signature of the fluid may evolve by fluid–rock interaction or through dilution with fluids trapped in isolated pores within the rock matrix. In transient systems, propagation of a shock wave through a zero porosity matrix may leave a residual porosity in its wake that decays asymptotically with time. Provided chemical processes such as crystallization, hydration or textural equilibration do not destroy the connectivity of this residual porosity, subsequent waves propagate in an environment with a finite background flux and porosity.

12.3. The e-fold effect

For typical geotherms, rock viscosities increase toward the surface by a factor of e, the natural log base, on a length scale $l_\eta \sim 1$–5 km, a scale comparable to the compaction lengths inferred in earlier studies of viscous compaction. Thus the local Deborah number, viscous compaction length and compaction time scale increase by an order of magnitude as a wave propagates $\sim 2.3\, l_\eta$. This implies that the vertical length scale for compaction is only the viscous compaction length if this length is less than l_η, otherwise the vertical length scale is l_η.

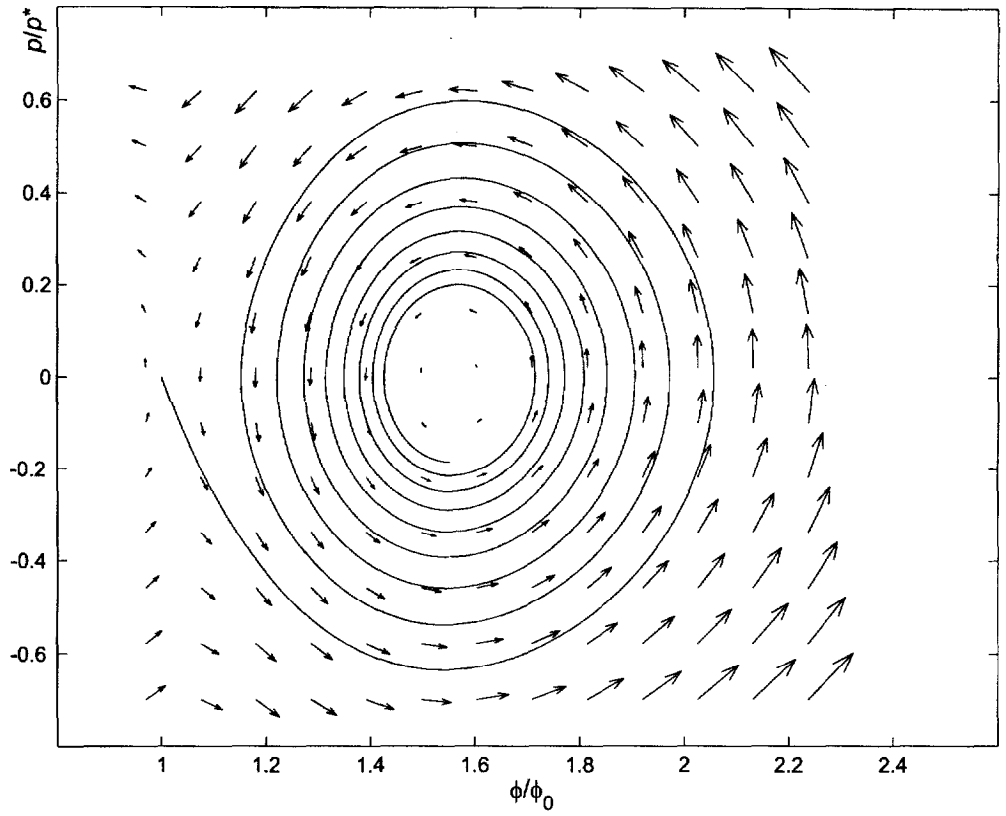

Figure 19. Pressure–porosity phase diagram for the stationary shock solution (*figure 18*) for flow of a compressible fluid in a viscous matrix. The spiral trace of the solution shows that the effect of fluid compressibility is to dampen the periodic and solitary solutions possible in a viscous matrix (*figure 6*). Because the trace begins in a counterclockwise direction from the shock front at $f = 1$ and $p = 0$, the wave-like structures within the shock decay to an elevated porosity above the shock front.

In this configuration, the horizontal length scale must be the local viscous compaction length of the unperturbed matrix. This length scale is important because it determines the scale on which lateral heterogeneities in compaction driven flow regimes can be maintained. For normal geothermal gradients this scale increases exponentially toward the surface, which suggests that lateral flow may occur on much greater length scales than inferred from simple models of viscous compaction.

The significance of the increase in the local Deborah number with depth is that there can be a rapid transition in the dominant mode of wave propagation. Thus, a metamorphic reaction may generate a sill-like viscous wave that initially propagates with a velocity on the order of ~1 km·My^{-1} [30]. The fluid pressure within the wave will rise as it propagates into the less viscous region of the crust. The increase in fluid pressure may then initiate a localized fluid pressure surge propagated by elastic deformation. Surge velocities three orders of magnitude faster than viscous wave velocities are feasible [1]. Such surges are a potential mechanism for breaching the lithostatic–hydrostatic fluid pressure transition [11] and generating seismicity [1]. Factors that mitigate against transient fluid pressure surges are the relatively large effective pressures required to initiate surges, an increase in permeability surfaceward, and plastic yielding. Variable viscosity has two profound consequences for the nature of wave propagation in the viscous limit, $De_\phi \ll 1$. (1) Viscous waves slow as they propagate and may become effectively stationary on a geologic time scale, an effect that may explain porosity-depth profiles and fluid compartmentalization in sedimentary basins. (2) A zero-dimensional perturbation forms oblate ellipsoidal waves, for which the aspect ratio, $\sim 1 + \delta/l_\eta$, increases exponentially toward the surface. Thus a subhorizontal fluid source, such as a melting or devolatilization reaction, will create sill-like one-dimensional waves if $l_\eta \leq \delta$. Local heterogeneities or thermal anomalies such as those that might be created by secondary convective overturn in the lithosphere or local heat advection by the fluid, can result in a rheologically upward weakening environment ($l_\eta < 0$). In these

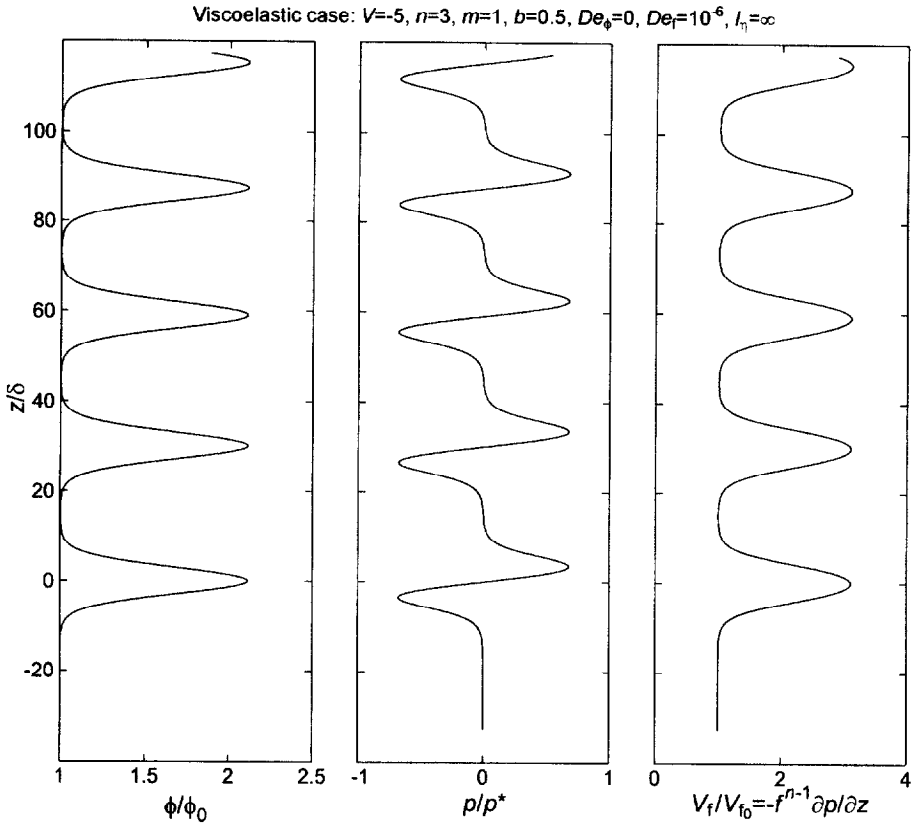

Figure 20. Analytic stationary solution for a shock developed by flow of a fluid with vanishing compressibility in a viscous matrix ($V = 5$, $n = 3$, $De_\phi = 0$, $b = 0.5$, $De_f = 10^{-6}$, $l_\eta = \infty$). The solution is a 'negative' shock (*figure 19*), but it is sensibly indistinguisable from a train of periodic solitary waves [30].

environments, prolate ellipsoidal waves or vertical fluid-filled channels would initiate from instabilities. These features may be the nuclei for self-propagating melt-filled cracks [33]. In this respect, the e-fold effect is remarkably similar to the effect of reactive transport which has been shown to be a potential mechanism for forming fluid channels [15].

13. Conclusion

We have ignored the roles of power-law rheologies and chemical source terms for porosity and fluid. These complications influence wave shape and the shock evolution, but we do not expect they would fundamentally alter our conclusions. The most important of these is that fluid flow in the viscous regions of the earth's lithosphere can be accomplished by self-propagating, isolated domains of fluid-filled porosity. It is particularly satisfying that it is only possible to reach this conclusion by employing a realistic rheological model. The length scale and shape of these porous domains is determined by the e-fold length, $l_\eta \sim 0.2$–5 km. The amplitude and velocity of these domains is likely to be highly variable, but is ultimately constrained by the consideration that fluid expulsion must approximately balance fluid production. We have concerned ourselves with understanding the fundamental aspects of porosity waves, rather than parameterization and applications of our model. Nonetheless, our results are of immediate relevance to a broad range of geological problems. While it is possible to dispute the origin of fluid compartments in sedimentary basins [37], the compartments are indisputable evidence for the existence of porosity waves in natural environments. Viscoplastic compaction-driven flow models not only reproduce such features [11], but also can explain the observations that in sedimentary basins: porosity varies more strongly with depth [i.e. equation (10)] than predicted by empirical models such as the Athy function [38], and that fluid compartments remain stationary on a geological timescale. In metamorphic environments, it has been inferred that fluid flow through rocks in which an interconnected fluid phase is texturally unstable occurs by

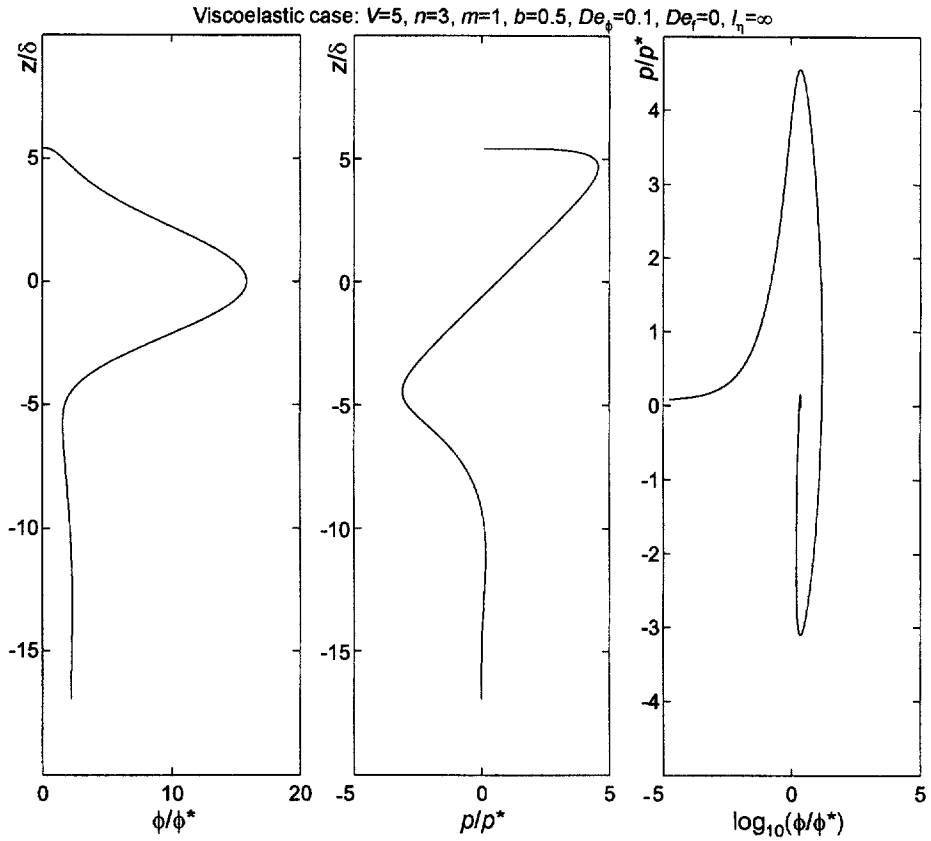

Figure 21. Analytic stationary solution for a shock developed by flow of an incompressible fluid (i.e. $De_f = 0$) in a viscoelastic matrix ($V = 1$, $n = 3$, $De_\phi = 0.1$, $b = 0.5$, $De_f = 0$, $l_\eta = \infty$) in the limit of zero porosity. The shock front is propagated by elastic deformation, the large wave-like structure behind the front is formed primarily by viscous deformation. Propagation is essentially limited by the rate at which viscous compaction drives fluid to the shock front. Because the background porosity is zero, the scaling given in equations (5) and (8) is no longer appropriate. To circumvent this problem, we scale shock phase velocity relative to a porosity ϕ^*, and define the compaction length accordingly. Similar shocks solutions are obtained for finite background porosity with the same rheological model. Discounting chemical effects, waves propagating through a zero-porosity matrix would propagate the geochemical signature of the fluid source region indefinitely.

the propagation of microcracks [39]. Viscoelastic porosity waves generated by metamorphic devolatilization are a mechanism by which this type of fluid flow could be sustained. These waves and the viscoelastic transition resulting from the e-fold effect are a potential source of the fluid pressure surges hypothesized by Rice [1] as a trigger for seismicity. The e-fold effect on fluid flow in a deformable matrix may be the key to the solution of two enigmatic problems, subhorizontal seismic reflectors [40] and the initiation of self-propagating melt or fluid-filled cracks [33, 34]. Seismic reflectors may represent subhorizontal accumulations of fluid resulting from a positive (i.e., normal) l_η-rheology, whereas the critical pressures required to initiate self-propagating fluid-filled cracks could be achieved within vertical fluid accumulations that are stabilized by a negative l_η-rheology. While we do not dismiss the potential importance of reactive transport in melt migration [15], we note that rheological models are better constrained and capable of reproducing the same phenomena. Regardless of the processes responsible for channelling pervasive asthenospheric melts, the e-fold effect is a simple mechanism that would explain the collection of channelled melt into sill-like features in the overlying lithosphere. It can be argued that the Deborah numbers characteristic of mantle environments are too low for elastic deformation to be a significant component of deformation propagated fluid flow, as we have advocated here. In defense of our thesis, we emphasize that the elastic modulus for porosity wave propagation is the tangential bulk modulus in tension. As rocks have vanishing cohesive strength at negative effective pressure, this modulus must also vanish under the conditions for viscous wave propagation. Therefore, the local Deborah

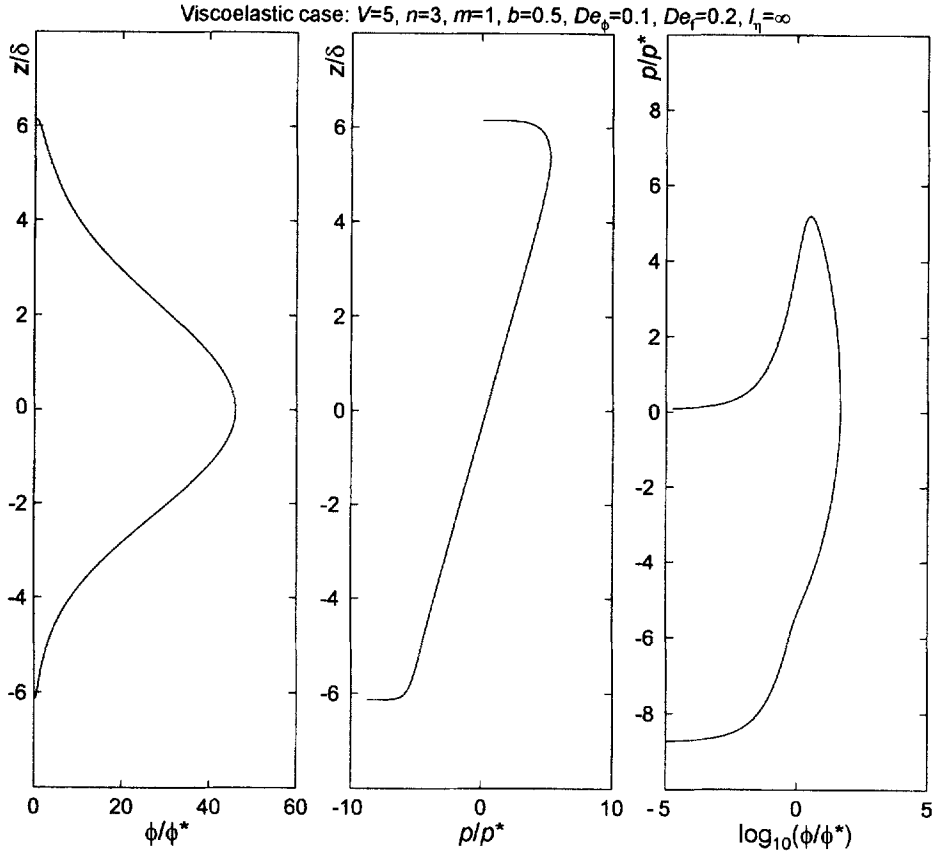

Figure 22. Analytic stationary solution for a shock developed by flow of a compressible fluid in a viscoelastic matrix ($V = 5$, $n = 3$, $De_\phi = 0.1$, $b = 0.5$, $De_f = 0.2$, $l_\eta = \infty$) in the limit of zero porosity. Scaling as in *figure 21*. Although the porosity wave appears to be a solitary wave, the pressure–porosity phase diagram shows that it is indeed a shock. The shape of the shock tip and tail are determined, respectively, by De_ϕ and De_f, with small Deborah numbers producing to more diffuse structures. Since the effective De_ϕ is inversely related to the tangential bulk modulus of the matrix in extension, which is potentially infinite, we expect that sharp shock fronts would develop in natural environments. In contrast, the effective De_f is related to the fluid compressibility and is likely to be $<<De_\phi$. Therefore, if such waves exist in nature, regardless of whether they are shocks or solitary waves, they are likely to have long, unstable tails.

number relevant for porosity wave propagation is essentially unbounded, even in high temperature environments such as the Earth's mantle.

Acknowledgements

We thank Jean-Pierre Burg for his editorial skill and almost unlimited patience, and Alexei Poliakov and Steve Miller for critical reviews. This work was undertaken as part of ETH-Forschungsprojekt 0-20-885-94.

14. Epilogue: flow channeling in a two-dimensional viscoplastic matrix

One-dimensional fluid flow in a viscoplastic matrix with either finite yield strength, or a finite but small viscosity for effective pressures exceeding a nominal yield strength, is similar with respect to time and length scales of fluid flow in a viscous matrix [11]. However, in contrast to the viscous case, one-dimensional viscoplastic porosity waves are not stabilized by an upward strengthening viscous rheology in two or three spatial dimensions, but rather decompose into vertically elongated waves or channels. The reason for this destabilization is that plastic yielding counteracts the e-fold effect in an upward strengthening rheology by weakening the matrix in the uppermost portion of a porosity wave and thus effectively eliminates the e-fold effect. If the variation in strength at the yield surface is large, as is normally the case for geological materials, then at the top of a wave small variations in the pieziometric fluid pressure gradient due to the gravitational field are sufficient to cause dilational deformation to propagate more rapidly vertically than laterally. The aspect ratio of two-

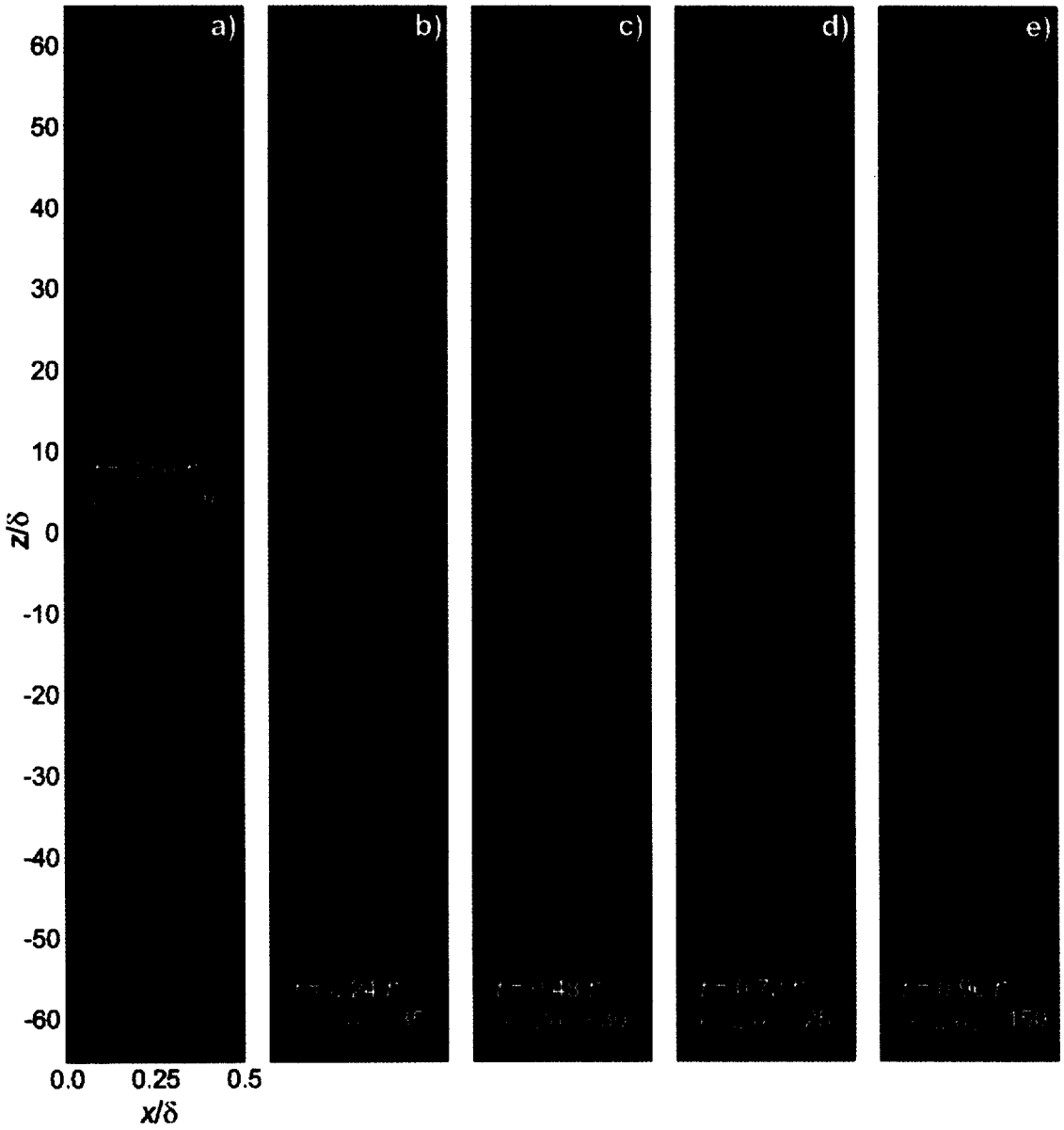

Figure 23. Transient two-dimensional porosity waves generated from a sill-like high porosity layer in a matrix with constant shear viscosity and plastic yielding at zero effective pressure. The horizontal scale is exaggerated by roughly a factor of 50. Plastic yielding is assumed to result in an effective shear viscosity three orders of magnitude less than the shear viscosity at positive effective pressure (i.e. $\eta_{yield}/\eta = 0.001$). **a**. The initial porosity distribution consists of a high porosity sill-like layer bounded by regions of low porosity. The average initial porosity in the sill-like layer is an order of magnitude greater than the background porosity. One-dimensional fluid flow is destabilized by 50 % white noise in the initial porosity values. **b**. Initial waves develop with an aspect ratio of ≈300, a vertical length scale and horizontal spacing comparable to the viscous compaction length and relatively large amplitudes ($\phi_{max}/\phi_0 > 20$). **c**. Porosity waves formed later in the compaction process exploit the partially compacted channels left in the wake of earlier waves. **d**. This process results in the formation of a continuous channel. **e**. The dynamics of the fluid supply determine whether flow occurs through pre-existing or new channels. Numerical models in which yield strength increases upward produce similar results except that the channels spread laterally to form sill-like porosity waves toward the surface.

and three-dimensional waves is determined by the manner in which plasticity manifests itself in the rheological behavior of the matrix. In the limit of ideal plastic yielding, wave aspect ratios (width/height) scale as $-p_{yield}/p^*$ for yield pressures of the order of, or less than, p^*. Alternatively, if the matrix has a finite shear viscosity,

Connolly and Podladchikov, Figure 23.

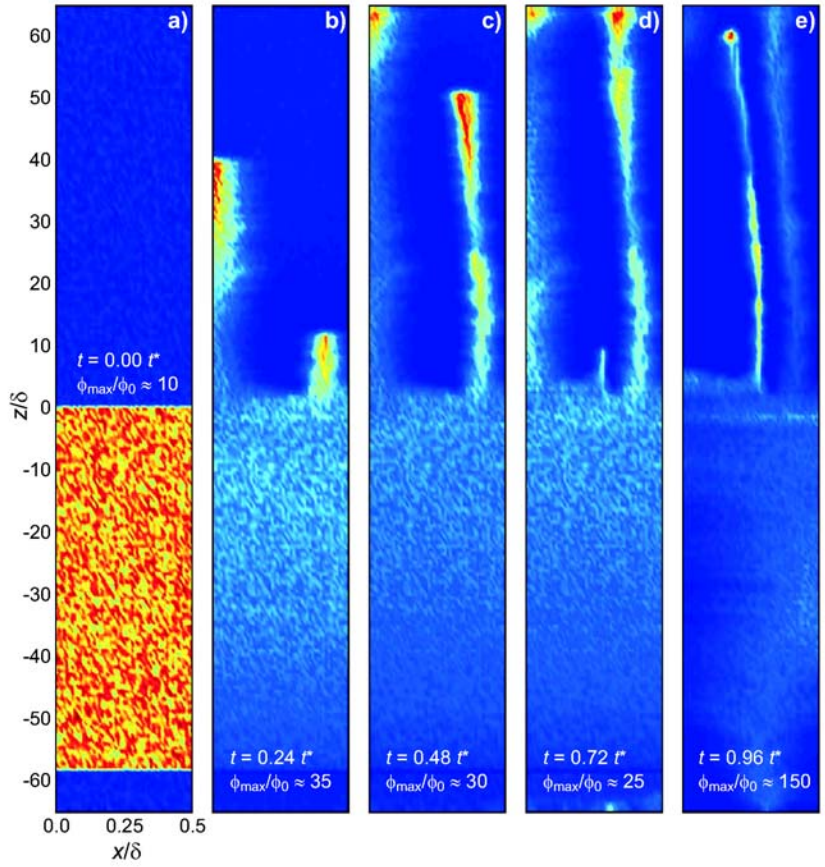

η_{yield}, at effective pressures below the yield pressure, wave aspect ratios vary as η_{yield}/η. These relationships imply that plasticity provides an efficient mechanism for channeling fluids (*figure 23*). From dimensional considerations, the spacing of the channels or waves in a viscoplastic matrix must occur with a horizontal spacing of $\sim\delta$. Likewise, the vertical length scale of channels or waves is $\sim\delta$ if $\delta << |l_\eta|$, and $|l_\eta|$ otherwise. In contrast to the e-fold effect in an upward weakening matrix, where wave aspect ratios increase with upward propagation limiting the vertical extent of any channelled flow regime, there is no fundamental dependence of aspect ratio on depth. More generally, it is to be expected that the nature of plastic yielding, and therefore the character of compaction driven fluid flow, will vary with depth. For example, the transition from channelled asthenospheric melt flow into sill-like horizontal porosity waves can be induced in numerical calculations if yield strength and matrix shear viscosity increase upward. This transition differs from the transition resulting from a change in the sign of the e-fold length in that the transformation from dike- to sill-like geometry occurs without an intermediate stage in which the waves are spheroidal. As porosity waves have radial symmetry in the absence of far-field deviatoric stresses, the term dike is used somewhat loosely here, however true three-dimensional dike like features could be generated with numerical models that incorporate such stress fields.

References

[1] Rice J.R., Fault stress states, pore pressure distributions, and the weakness of the San Andreas fault, in: Evans B., Wong T.-F. (Eds.), Fault Mechanics and Transport Pro-perties of Rocks, Academic Press, NY, 1992, pp. 475–503.

[2] Richter F.M., McKenzie D., Dynamical models for melt segregation from a deformable rock matrix, J. Geol. 92 (1984) 729–740.

[3] Scott D., Stevenson D., Magma solitons, Geophys. Res. Lett. 11 (1984) 1161–1164.

[4] Fowler A., A mathematical model of magma transport in the asthenosphere, Geophys. Astrophys. Fluid Dyn. 33 (1984) 155–190.

[5] Gueguen Y., Palciauskas V.V., Introduction to the Physics of Rocks, Princeton Univ. Press, Princeton, N.J., 1994.

[6] McKenzie D., The compaction of igneous and sedimentary rocks, J. Geol. Soc. Lond. 144 (1987) 299–307.

[7] Kooi H., Insufficiency of compaction disequilibrium as the sole cause of high pore fluid pressures in pre-Cenozoic sediments, Basin Research 9 (1997) 227–241.

[8] Rutter E.H., The kinetics of rock deformation by pressure solution, Phil. Trans. R. Soc. London 283A (1976) 203–219.

[9] Gratz A.J., Solution transfer compaction of quartzites—progress toward a rate law, Geology 19 (1991) 901–904.

[10] Dewers T., Hajash A., Rate laws for water-assisted compaction and stress-induced water-rock interaction, J. Geophys. Res. 100 (1995) 13093–13112.

[11] Connolly J.A.D., Compaction-driven fluid compartmentalization in sedimentary basins: a numeric model, Tectonphysics (1998) in review.

[12] Scott D., Stevenson D., Magma ascent by porous flow. J. Geophys. Res. 91 (1986) 9283–9296.

[13] Stevenson D., Spontaneous small-scale melt segregation in partial melts undergoing deformation, Geophys. Res. Lett. 16 (1989) 1067–1070.

[14] Wiggins C., Spiegelman M., Magma migration and magmatic solitary waves in 3D, Geophys. Res. Lett. 22 (1995) 1289–1292.

[15] Aharanov E., Spiegelman M., Coleman P., Three-dimensional flow and reaction in porous media: implications for the Earth's mantle and sedimentary basins, J. Geophys. Res. 102 (1997) 14821–14834.

[16] Nye J.F., The flow law of ice from measurements in glacier tunnels, laboratory experiments and the Jungfraufirn borehole experiment Proc. R. Soc. Lond. 219A (1953) 477–489.

[17] Ashby M.F., The modeling of hot isostatic pressing, in: Garvare T. (Ed.), Proceedings HIP: Hot Isostatic Pressing—Theories and Applications, Centek, Lulea, Sweden, 1997, pp. 29–40.

[18] Kohlstedt D.L., Evans B., Mackwell S.J., Strength of the lithosphere: constraints imposed by laboratory experiments, J. Geophys. Res. 100 (1996) 17587–17602.

[19] Holness M.B., Surface chemical controls on pore–fluid connectivity in texturally equilibrated materials, in: Jamtveit B.J., Yardley B.W.D. (Eds.), Fluid flow and transport in rocks, Chapman and Hall, London, 1997, pp. 149–170.

[20] Gavrilenko P., Gueguen Y., Fluid overpressures and pressure solution in the crust, Tectonophysics 21 (1993) 91–110.

[21] Barenblatt G.I., Scaling, Self-similarity, and Intermediate Asymptotics, Cambridge University Press, Cambridge, 1996.

[22] McKenzie D., The generation and compaction of partially molten rock, J. Petrol. 2 (1984) 713–765.

[23] Barcilon V., Richter F.M., Non-linear waves in compacting media, J. Fluid. Mech. 164 (1986) 429–448.

[24] Spiegelman M., Flow in deformable porous media. Part 1. Simple analysis, J. Fluid. Mech. 247 (1993) 17–38.

[25] Khodakovskii G., Rabinowicz M., Genthon P., Ceuleneer G., 2D modeling of melt percolation in the mantle: the role of a melt dependent mush viscosity, Earth Planet. Sci. Lett., 1995.

[26] Bethke C.M., A numerical model of compaction-driven groundwater flow and heat transfer and its application to the paleohydrology of intracratonic sedimentary basins, J. Geophys. Res. 90 (1985) 6817–6628.

[27] Van Balen R., Cloetingh S., Tectonic control of the sedimentary record and stress-induced fluid flow: constraints from basin modelling, in: Parnell J. (Ed.), Geofluids: Origin, Migration and Evolution of Fluids in Sedimentary Basins, Geol. Soc. Spec. Pub., 1994, pp. 9–26.

[28] Poliakov A., Cundall P., Podladchkov Y., Lyakhovsky V., An explicit inertial method for the simulation of visco-elastic flow: an evaluation of elastic effects on diapiric flow in two- and three-layer models, in: Stone D.B., Runcorn S.K. (Eds.), Flow and Creep in the Solar System: Observations, Modeling and Theory, Kluwer Academic Publishers, Amsterdam, 1993, pp. 175–195.

[29] David C., Wong T.-F., Zhu W., Zhang J., Laboratory measurements of compaction induced permeability change in porous rocks: implications for the generation and maintenance of pore pressure excess in the crust, Pure Appl. Geophys. 143 (1994) 425–456.

[30] Connolly J.A.D., Devolatilization-generated fluid pressure and deformation-propagated fluid flow during regional metamorphism, J. Geophys. Res. 102 (1997) 18149–18173.

[31] Peaceman D.W., Rachford H.H., The numerical solution of parabolic and elliptical differential equations, Journal of the Society for Industrial and Applied Mathematics 3 (1955) 28–41.

[32] Spiegelman M., Flow in deformable porous media. Part 2. Numerical analysis—the relationship between shock waves and solitary waves, J. Fluid. Mech. 247 (1993) 17–38.

[33] Rubin R.M., Propagation of magma-filled cracks, Ann. Rev. of Earth Planet. Sci. 23 (1995) 287–336.

[34] Nakashima Y., Transport model of buoyant metamorphic fluid by hydrofracturing in leaky rock, J. Metamorph. Geol. 13 (1995) 727–736.

[35] Whitham G.B., Linear and Nonlinear Waves, Wiley, New York, 1974.

[36] Lyakhovsky V., Podladchikov Y., Poliakov A., A rheological model of a fractured solid, Tectonophysics 226 (1993) 187–198.

[37] Hunt J.M., Generation and migration of petroleum from abnormally pressured fluid compartments, Amer. Assoc. Petr. Geol. 74 (1990) 1–12.

[38] Biot, Odé, Theory of gravity instability with variable overburden and compaction, Geophysics 30 (1965) 213–227.

[39] Bickle M.J., Baker J., Advective-diffusive troansport of isotopic fronts: an example from Naxos, Greece, Earth Planet. Sci. Lett. 97 (1990) 78-93.

[40] Hyndman R.D., Dipping seismic reflectors, electrically conductive zones, and trapped water in the crust over a subducting plate, J. Geophys. Res. 93 (1988) 13391–13405.

[41] Szalay A., Possibilities of the reconstruction of basin evolution in the prediction of hydrocarbon prospects, Hungarian Academy of Sciences, Budapest, 1982.

[42] Shimizu I., Kinetics of pressure solution creep in quartz; theoretical considerations, Tectonophysics 245 (1995) 121–134.

[43] Gleason G.C., Tullis J., A flow law for dislocation creep of quartz aggregates determined with the molten salt cell, Tectonophysics 247 (1995) 1–23.

Fig13 Connolly&Podladchikov

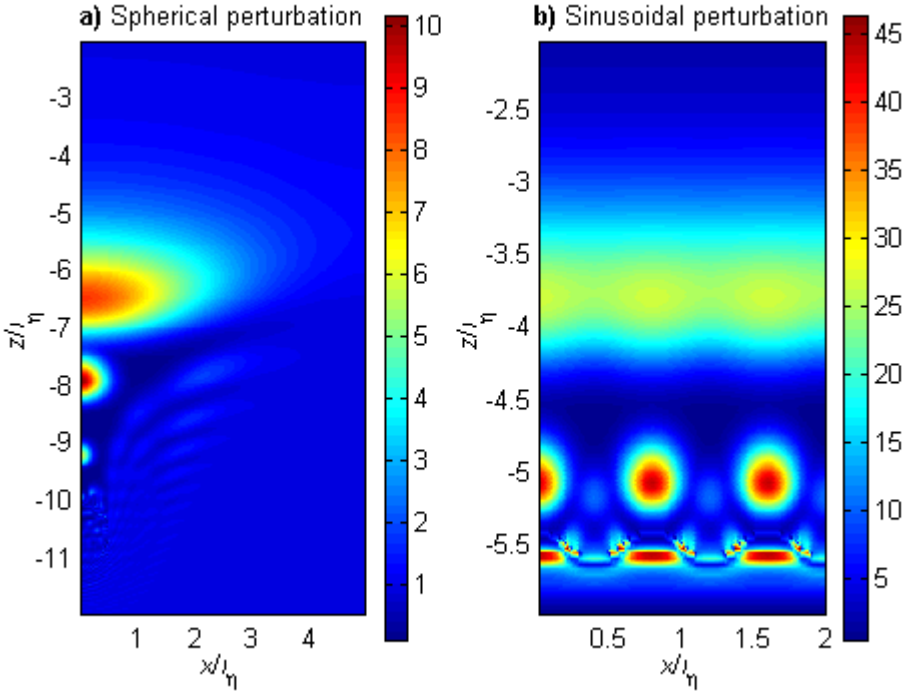

Fig17 Connolly&Podladchikov

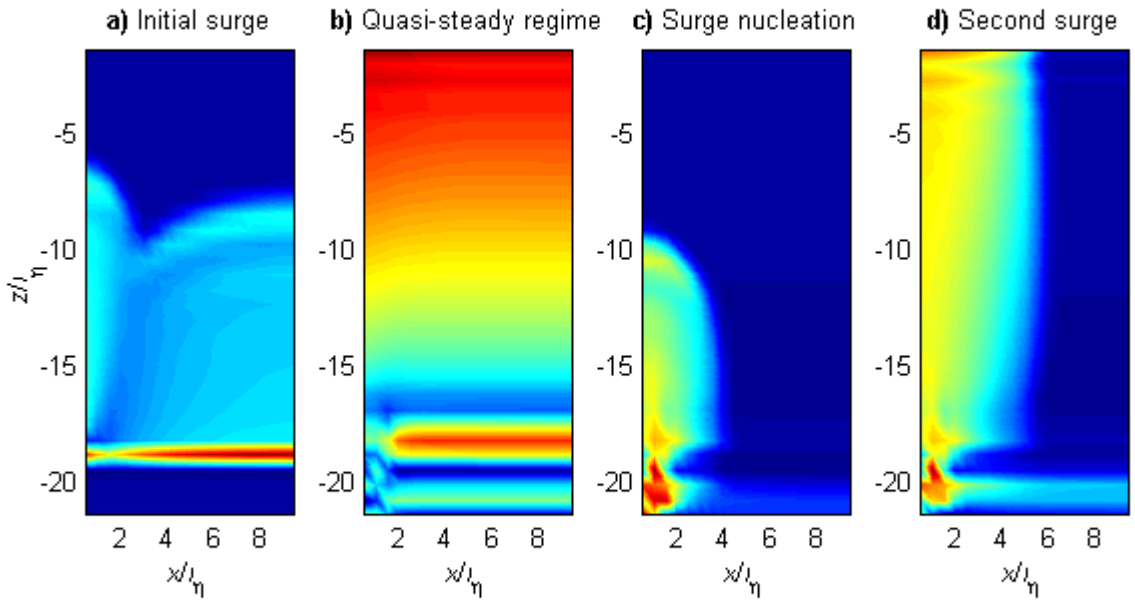

Connolly and Podladchikov, Figure 23.

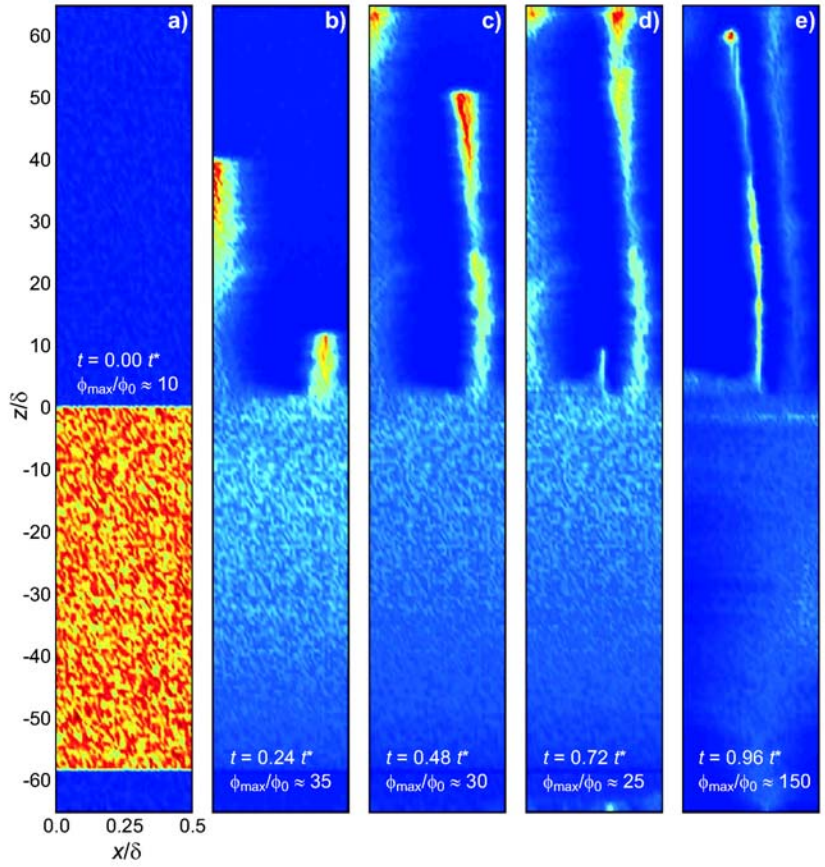

Erratum for Connolly and Podladchikov, Geodinamica Acta, 11:55-84, 1998:

Eq 12 last factor should read $(z - z_0)/l$ rather than $(z - z_0)/l$

Figures 1 and 12 should be replaced by the versions appended here.

Figure 1.

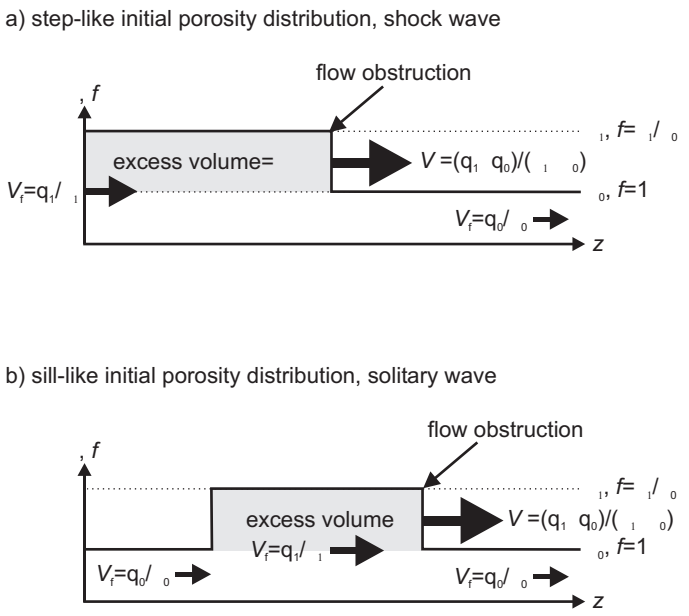

Figure 12.